

Conformalized Decision Risk Assessment

Wenbin Zhou

Heinz College of Information Systems and Public Policy, Carnegie Mellon University, wenbinz2@andrew.cmu.edu

Agni Orfanoudaki

Saïd Business School, University of Oxford, agni.orfanoudaki@sbs.ox.ac.uk

Shixiang Zhu

Heinz College of Information Systems and Public Policy, Carnegie Mellon University, shixianz@andrew.cmu.edu

In many operational settings, decision-makers must commit to actions before uncertainty resolves, but existing optimization tools rarely quantify how consistently a chosen decision remains optimal across plausible futures. This paper introduces CREDO—Conformalized Risk Estimation for Decision Optimization, a distribution-free framework that quantifies the probability that a prescribed decision remains (near-)optimal across realizations of uncertainty. CREDO reformulates decision risk through the inverse feasible region—the set of outcomes under which a decision is optimal—and estimates its probability using inner approximations constructed from conformal prediction balls generated by a conditional generative model. By calibrating each ball to lie entirely within the inverse feasible region, CREDO obtains finite-sample valid lower bounds on decision optimality without parametric assumptions. The method avoids the conservatism of worst-case robust optimization, is compatible with modern generative models, and applies broadly to convex optimization problems. We establish theoretical validity guarantees, develop efficient computational procedures, and demonstrate through extensive numerical experiments that CREDO provides accurate, interpretable, and reliable assessments of decision reliability in both synthetic and application-motivated settings.

Key words: Conformal prediction, Inverse optimization, Risk analysis, Human-centered decision-making

1. Introduction

Organizations routinely make consequential decisions in the presence of substantial uncertainty (Kochenderfer 2015). Utilities must plan infrastructure upgrades without knowing future load growth or the intensity of extreme weather events (Chen et al. 2025); hospitals must allocate limited staff and beds before patient needs are realized (Kim and Mehrotra 2015); and public agencies

must design policies whose impacts depend on uncertain behavioral and socioeconomic responses (Zhu et al. 2022). In such settings, decision-makers are tasked with selecting the best action by solving an optimization problem that will remain effective across a range of possible scenarios. Classical approaches address this challenge by representing uncertainty through forecasts or sampled scenarios and subsequently optimizing with respect to this surrogate representation. Two common instantiations of this paradigm are predict-then-optimize (Bertsimas and Kallus 2020, Elmachtoub and Grigas 2022), where decisions are optimized against a point forecast, and scenario-based stochastic programming (Bertsimas et al. 2018), where decisions are chosen to minimize expected cost across empirical samples. These tools have formed the backbone of prescriptive analytics in operations and have been successfully deployed across numerous application domains (Bertsimas et al. 2021, Tian et al. 2023).

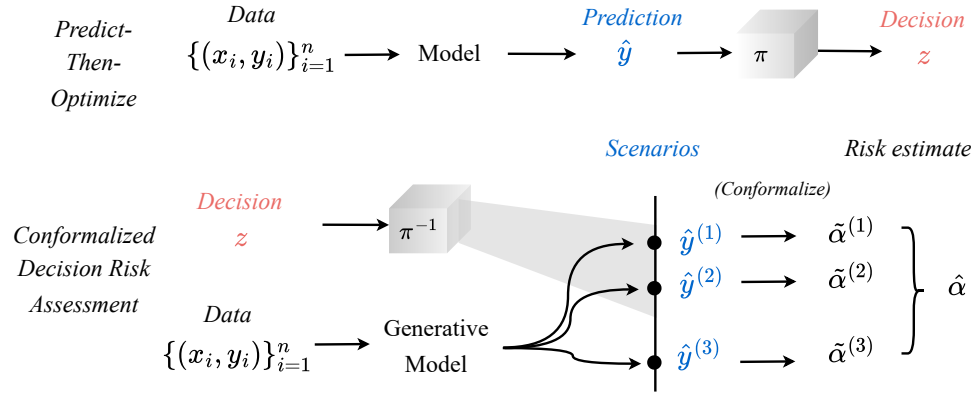
Despite their widespread use, these approaches provide a limited view of the decision landscape. Many operational problems admit multiple actions that perform nearly equivalently across plausible realizations of uncertainty (Topkis 1998, Bertsimas and Sim 2004). For example, several investment plans may harden the electric grid to similar degrees under different storm patterns (Lombardi et al. 2025), or multiple staff schedules may achieve comparable service quality across demand scenarios (DeCarolis 2011, Palmintier 2014). Yet classical optimization pipelines return only a single recommended action, offering little visibility into whether this choice is robust or whether alternative decisions are nearly as effective (Li and Zhu 2024, Zhang et al. 2025). As a result, decision-makers must often rely on informal heuristics or domain intuition to assess the reliability of the prescribed solution and to understand how frequently it would remain optimal as the environment varies (Delarue et al. 2025). This gap between the deterministic nature of traditional models and the practical need to evaluate the reliability of decisions highlights the need for new rigorous tools that more directly quantify decision reliability.

Our work addresses this gap by adopting a complementary perspective to the established literature. Rather than collapsing uncertainty into a single deterministic representation, we focus on *quantifying the likelihood that a given decision remains (near-)optimal under different realizations of the environment*. The central question shifts from “What does the model recommend?” to “How reliably will this prescribed decision perform under varying conditions?” Under this view, analytical tools serve not as automatic decision engines but as decision-support systems that assess how robust a candidate solution is to underlying data variability. Such information is valuable in operational human-in-the-loop contexts where human judgment, regulatory oversight, or organizational risk tolerance ultimately shape the chosen action (Dietvorst et al. 2018, Grand-Clément and Pauphilet 2024). By quantifying the reliability of a decision, the framework provides interpretable evidence that supports accountability, stakeholder communication, and more informed strategic planning.

To operationalize this perspective, we introduce CREDO—Conformalized Risk Estimation for Decision Optimization, a framework that quantifies, for any candidate decision, a distribution-free lower bound on the probability that it remains (near-)optimal (see Figure 1 for an illustration). The proposed approach integrates inverse optimization (Chan et al. 2025) with distribution-free uncertainty quantification via conformal prediction (CP) (Angelopoulos and Bates 2021). The core challenge is to evaluate the likelihood that an uncertain scenario falls within the decision’s inverse feasible region, namely the set of scenarios under which that decision remains optimal or near-optimal, and directly characterizing this region is generally intractable due to its implicit and complex geometry.

CREDO circumvents this challenge by constructing inner approximations of the inverse feasible region using multiple CP balls generated from a conditional generative model. Each ball serves as a finite-sample valid prediction region for the outcome. By shrinking the radius until the ball fits entirely inside the inverse feasible region, we obtain a certified lower bound on the decision’s

Figure 1 Illustration of Conformalized Decision Risk Assessment (CREDO) compared against Prediction-Then-Optimize (PTO).



Note. For a given candidate decision z and dataset $\{(x_i, y_i)\}_{i=1}^n$, CREDO aims to estimate the decision risk, which is defined as the probability of z to be suboptimal. CREDO finds the inverse feasible region using inverse optimization π^{-1} , and uses a generative model to simulate multiple scenarios, which are then calibrated to produce the conformalized risk estimate $\hat{\alpha}$.

optimality probability. Aggregating these calibrated bounds yields a distribution-free, finite-sample valid estimator of decision risk. CREDO is compatible with modern generative forecasting models, supports multiple conformal radius constructions, and applies broadly to convex decision problems. We establish theoretical validity for the estimator, develop efficient computational procedures, and demonstrate through extensive numerical experiments that CREDO provides accurate, interpretable, and reliable assessments of decision reliability across both synthetic and application-driven settings. In what follows, we summarize the key contributions of our work:

- **Problem Formulation:** We formulate the decision risk assessment as estimating the probability that a candidate decision remains (near-)optimal under uncertainty. By expressing this probability through inverse feasible regions, we convert an otherwise intractable evaluation problem into a tractable estimation task, revealing a fundamental link between inverse optimization and distribution-free uncertainty quantification.
- **CREDO Framework:** We introduce CREDO, a distribution-free framework based on CP that delivers finite-sample valid lower bounds on decision optimality, and establish marginal conservativeness, asymptotic consistency, and accuracy guarantees.

- **Computational Algorithm:** We derive a closed-form estimator for linear programs and develop an efficient computational procedure applicable to general convex optimization problems.
- **Empirical Validation:** Through controlled synthetic experiments and a real-world power grid planning application with 1,700+ solar installations, we verify CREDO’s theoretical guarantees and demonstrate its practical advantages. Our method achieves 100% empirical validity under conservative radius choices, superior true positive rates (up to 78.75% improvement over baselines), and consistently selects decisions with higher empirical confidence rankings than existing prescriptive methods.

The remainder of this paper is organized as follows. Section 2 reviews the related literature and positions our contributions. Section 3 formalizes the decision risk assessment problem and provides motivating examples. In Section 4, we present the CREDO methodology, combining inverse optimization with generative CP. Section 5 establishes theoretical guarantees including validity, consistency, and true positive rate analysis. Section 6 details the proposed computational implementation of CREDO, while Section 7 demonstrates its effectiveness through synthetic and real-world experiments. Section 8 concludes with discussions of implications and future work. Technical proofs and additional details are in the Electronic Supplement.

2. Related Work

Our work draws from and contributes to four distinct research streams: *(i)* decision-making under uncertainty in operations research, *(ii)* distribution-free uncertainty quantification through CP, *(iii)* inverse optimization for understanding decision structures, and *(iv)* human-algorithm collaboration in decision support systems. In what follows, we position the CREDO approach relative to these lines of research.

Classical approaches to optimization under uncertainty can be categorized by their treatment of unknown parameters. Stochastic optimization seeks decisions that minimize the expected value of

the objective function across probabilistic scenarios, typically implemented through sample average approximation over historical data (Shapiro et al. 2021, Kleywegt et al. 2002, Lan et al. 2025). The predict-then-optimize paradigm offers an alternative by first estimating unknown parameters via predictive models, then solving the resulting deterministic optimization problem (Bertsimas and Kallus 2020, Elmachtoub and Grigas 2022). Acknowledging that probability distributions themselves may be misspecified, robust optimization is employed to hedge against worst-case realizations within specified uncertainty sets (Bertsimas and Thiele 2006, Ben-Tal and Nemirovski 2002). Distributionally robust optimization generalizes this concept further, considering worst-case probability distributions rather than point realizations, thereby balancing conservatism with statistical plausibility (Delage and Ye 2010, Rahimian and Mehrotra 2022). Recognizing that prediction errors can compound when models are trained separately from their downstream use, decision-focused learning trains predictive models end-to-end by differentiating through the optimization layer, directly minimizing downstream decision costs rather than prediction errors (Amos and Kolter 2017, Mandi et al. 2024). While these prescriptive paradigms effectively recommend decisions, our work adopts a parallel goal: rather than *prescribing* a decision, we focus on *auditing* decisions by providing a quantitative, data-driven assessment of the risk associated with taking a given decision. This perspective complements existing decision-prescription methods and even human judgment by adding an additional layer of transparency and accountability, thereby supporting more reliable and defensible decision-making.

Methodologically, our work builds upon the CP literature, a distribution-free approach for uncertainty quantification through calibrated prediction sets (Shafer and Vovk 2008, Vovk et al. 2005). We highlight two strands of recent research that are particularly relevant to our work. First, generative conformal methods draw multiple samples from generative models to construct both the calibration sets and the resulting CP regions, thus significantly improving efficiency (*i.e.*, tightness

of the prediction sets) especially when the data distribution is highly complex or dispersed (Zheng and Zhu 2024, Zhou et al. 2024). Second, inverse CP estimates miscoverage rates for fixed prediction sets by identifying the smallest miscoverage level at which conformal regions are contained within the target set (Prinster et al. 2023, Singh et al. 2024). Advances in e -value CP strengthen this approach by enabling post-hoc selection of the miscoverage rate while preserving finite-sample validity at the theoretical level (Vovk 2025, Gauthier et al. 2025b). Our algorithm synthesizes both advances by leveraging generative models to enhance decision-risk estimation accuracy and subsequently employing generalized inverse CP to assess the decision risk. However, we emphasize that our problem setting is fundamentally different and cannot be addressed by direct application of these methods. Substantive reformulation is required to adapt their underlying ideas to the decision-auditing context.

Our work also connects to inverse optimization (IO), which seeks to infer the unknown parameters of an optimization problem from observed solutions (Ahuja and Orlin 2001, Chan et al. 2025, Aswani et al. 2018). Recent work on Conformal-IO combines IO with CP to prescribe robust decisions by first estimating decision-makers’ preference parameters from observed choices and then applies robust forward optimization using CP to construct an uncertainty set over these parameters (Lin et al. 2024, Chan et al. 2024). While we similarly integrate IO and CP, our learning setting fundamentally differs. We assume access to samples of the unknown parameters rather than the actual decisions. This leads us to employ inverse CP to assess decision reliability (Singh et al. 2024) rather than forward CP to prescribe decisions. Our focus on evaluation rather than prescription distinguishes our approach from Conformal-IO’s goal of generating policy recommendations. While efficient IO algorithms exist for structured problems like linear, integer, and convex programs (Tavashioğlu et al. 2018, Schaefer 2009, Iyengar and Kang 2005), the lack of a unified framework for general IO leads to the adoption of structured formulations for tractability (Chan et al. 2024). This motivates

our focus on linear models as part of our theoretical analysis, allowing us to derive an efficient closed-form solution for the proposed implementation algorithm.

Finally, our research complements a growing line of work on human-algorithm collaboration in decision-making under uncertainty (Kiyani et al. 2025, Cortes-Gomez et al. 2024, Hullman et al. 2025, Cresswell et al. 2024). Unlike prior work that prescribes decisions, we leverage CP techniques to audit and assess the risk of candidate decisions, supporting human judgment through evaluation rather than recommendation. Additionally, our work contributes to the growing literature on the use of generative models to optimize in hybrid systems where human experts receive algorithmic advice (Grand-Clément and Pauphilet 2024, Ibrahim et al. 2021, Orfanoudaki et al. 2022). By producing a diverse set of plausible decisions, generative algorithms can act as advisory tools, thus promoting exploration and helping users develop more effective decision strategies (Ajay et al. 2022, Li and Zhu 2024).

Aligned with this perspective, our approach encourages decision-makers to evaluate alternatives beyond standard prescriptive recommendations, revealing risks and improvements that the nominal optimal decision alone may obscure. This emphasis on expanding the space of considered decisions is a central conceptual contribution of our work.

3. Problem Setup

We consider a general parametric decision-making model in which the decision is determined as the (near-)optimal solution to a constrained optimization problem under an observed scenario $y \in \mathcal{Y}$ (e.g., demand, price, or system load). Formally, we define the ϵ -optimal decision rule as

$$\pi_\epsilon(y) := \arg \min_{\epsilon, z \in \mathcal{Z}} f(z; y), \quad (1)$$

where f denotes the objective function (e.g., cost, delay, or loss), and \mathcal{Z} denotes the feasible region. We assume that \mathcal{Z} is nonempty and compact, and that $f(\cdot; y)$ is continuous and convex in z for

each y , ensuring the set $\pi_\epsilon(y)$ is non-empty for every $y \in \mathcal{Y}$. The operator $\arg \min_\epsilon$ generalizes the standard $\arg \min$ to allow a tolerance level $\epsilon \geq 0$, defined as:

$$\arg \min_\epsilon f(z) := \left\{ z \mid f(z) \leq \inf_{z'} f(z') + \epsilon \right\}.$$

In particular, setting $\epsilon = 0$ recovers the *exact optimal decision rule*. Throughout the manuscript, we suppress the subscript ϵ when no ambiguity arises, writing $\pi(y)$ for $\pi_\epsilon(y)$.

In many operational contexts, the realized scenario y is unobserved at the time of decision-making. Let $z \in \mathcal{Z}$ denote a prescribed (implemented) decision—potentially produced by a human operator, heuristic policy, or black-box model—made without access to the true realization of $Y \sim \mathcal{P}_Y$. This setup captures a common class of practical decision environments where actions are based on implicit or subjective beliefs about the underlying uncertainty rather than a fully specified probabilistic model.

Our objective is to assess how well a prescribed decision z aligns with the (unknown) optimal response under the true realization of Y . Formally, this quantity is expressed as the probability that z belongs to the (near-)optimal decision set $\pi(Y)$, *i.e.*, $\mathbb{P}\{z \in \pi(Y)\}$, where the probability is taken with respect to $Y \sim \mathcal{P}_Y$. This captures how frequently the prescribed decision coincides with an (approximately) optimal choice across possible realizations. Since the distribution \mathcal{P}_Y is typically unknown and only limited samples $\mathcal{D} = \{Y_i\}_{i=1}^n$ are available, this probability cannot be estimated precisely. We therefore focus on its data-driven lower bound $1 - \alpha(z)$ defined as

$$\mathbb{P}\{z \in \pi(Y)\} \geq 1 - \alpha(z). \quad (2)$$

The quantity $1 - \alpha(z)$ serves as a conservative and distribution-free optimality certificate, providing a guaranteed confidence level that the prescribed decision z is (near-)optimal under the true, unknown distribution \mathcal{P}_Y .

In the general setting, the quantities in (2) may depend on additional contextual covariates $X \in \mathcal{X}$, such as spatial, temporal, or environmental factors that influence the realization of Y . Accordingly, both the decision set $\pi(Y)$ and the confidence function $\alpha(z)$ can be defined conditionally on X , reflecting the dependence of the outcome distribution $\mathcal{P}_{Y|X}$ on its context. Also, the available data take the form $\mathcal{D} = \{(Y_i, X_i)\}_{i=1}^n$ in this case, capturing paired observations of outcomes and their associated covariates. For clarity of exposition, in the remainder of the paper, we omit the explicit dependence on X and focus on the marginal representation.

3.1. Motivating Examples

We provide two illustrative examples to demonstrate how the proposed problem setup applies to different decision-making contexts, ranging from simple binary decisions to complex resource allocation problems.

EXAMPLE 1 (STYLIZED UMBRELLA-CARRYING DECISION). A human decision-maker decides whether to carry an umbrella without checking the weather. Let $z \in \{0, 1\}$ denote the decision ($z = 1$: carry; $z = 0$: not carry) and $y \in \{0, 1\}$ denote the realized weather ($y = 1$: rain; $y = 0$: no rain). The feasible set is $\mathcal{Z} = \{0, 1\}$, and the objective function is a hinge-type misclassification cost:

$$f(z; y) = \begin{cases} 1, & \text{if } z \neq y \text{ (mismatch between decision and weather),} \\ 0, & \text{otherwise,} \end{cases} \quad \text{or simply } f(z; y) = \mathbb{1}\{z \neq y\}.$$

In this example, the human decision-maker acts based on an implicit perception of local weather patterns Y . The chosen decision z thus reflects the decision-maker's subjective belief about the likelihood of rain—carrying an umbrella if rain is perceived as more probable, and abstaining otherwise. Our goal is to assess whether this private knowledge aligns with the true local weather distribution by evaluating, through empirical data, how frequently the prescribed decision coincides with the optimal decision under the observed realizations of Y .

EXAMPLE 2 (CLINICAL TRIAGE). A clinician must allocate limited treatment resources under time pressure without reviewing complete patient records. Let there be d patients, and define the decision $\mathbf{z} = (z_1, \dots, z_d) \in \{0, 1\}^d$, where $z_j = 1$ if patient j receives treatment, subject to a capacity constraint $\sum_{j=1}^d w_j z_j \leq B$ (e.g., limited ICU beds, clinician time, or medication supply), with $w_j > 0$ denoting resource use of patient j and $B > 0$ the available budget. Let $\mathbf{x} = (x_1, \dots, x_d)$ represent observable clinical covariates, and $\mathbf{y} = (y_1, \dots, y_d)$ with $y_j \geq 0$ the realized benefit of treating patient j given x_j . The feasible region and objective function are defined as

$$\mathcal{Z} = \left\{ \mathbf{z} \in \{0, 1\}^d : \sum_{j=1}^d w_j z_j \leq B \right\}, \quad f(\mathbf{z}; \mathbf{y}) = - \sum_{j=1}^d y_j z_j.$$

In this more realistic setting, the clinician makes treatment decisions based on incomplete information or heuristic prioritization, such as triage scores or observable symptoms (Parenti et al. 2014). The prescribed decision vector \mathbf{z} encodes the clinician’s implicit belief about which patients are most likely to benefit given the resource constraint. We aim to evaluate whether such implicit prioritization aligns with the optimal clinical decisions suggested by data, by comparing the prescribed allocation with the optimal allocation derived from empirical patient records.

4. The CREDO Framework

We now present our method, which adapts the distribution-free uncertainty quantification framework of CP (Angelopoulos and Bates 2021) to estimate decision risk through calibrated inverse feasible regions.

4.1. Preliminary: Conformal Prediction

CP (Papadopoulos et al. 2002) is a model-agnostic framework for uncertainty quantification that delivers finite-sample valid prediction regions under the exchangeability assumption:

ASSUMPTION 1 (Exchangeability). *The calibration data $\{(X_i, Y_i)\}_{i=1}^n$ and the test point (X, Y) are exchangeable. That is, the joint distribution of $(X_1, Y_1), \dots, (X_n, Y_n), (X, Y)$ is invariant under any permutation of these $(n + 1)$ pairs.*

Let the calibration dataset be $\mathcal{D} = \{(X_i, Y_i)\}_{i=1}^n$, drawn from an arbitrary joint distribution over $\mathcal{X} \times \mathcal{Y}$. For a user-specified miscoverage rate α , the objective is to construct a prediction set $C(\cdot; \alpha)$ such that

$$\mathbb{P}\{Y \in C(X; \alpha)\} \geq 1 - \alpha, \quad (3)$$

where the probability is taken jointly over the randomness in the test point (X, Y) and the calibration data \mathcal{D} . This requirement is referred to as marginal validity.

Split CP (Papadopoulos et al. 2002) provides a practical and computationally efficient method for achieving the guarantee in (3). The procedure begins by training a prediction model $g : \mathcal{X} \rightarrow \mathcal{Y}$ using data independent of the calibration set. We then specify a nonconformity score function $l : \mathcal{X} \times \mathcal{Y} \rightarrow \mathbb{R}$, which quantifies how atypical a candidate label is relative to the model's prediction; for instance, one may take $l(x, y) = \|y - g(x)\|_2$. Given the calibration dataset, we compute the corresponding nonconformity scores

$$L_i = l(X_i, Y_i), \quad \forall i = 1, \dots, n.$$

These scores determine how large a deviation from the model is acceptable in order to guarantee the desired coverage. For any $\alpha \in [1/(n+1), 1)$, we define the adjusted empirical quantile as

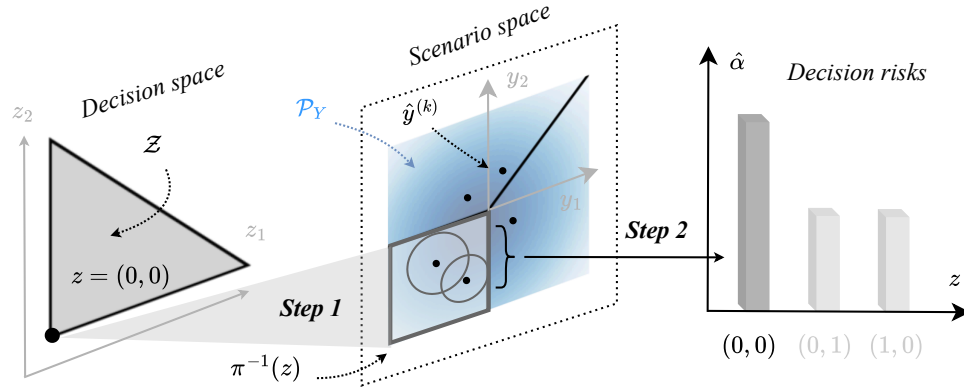
$$\hat{Q}(\alpha) = \inf \left\{ l \in \mathbb{R} : \hat{F}_n(l) \geq \frac{\lceil (n+1)(1-\alpha) \rceil}{n} \right\}, \quad \text{where} \quad \hat{F}_n(l) = \frac{1}{n} \sum_{i=1}^n \mathbb{1}\{L_i \leq l\}.$$

This quantile defines the prediction region:

$$C(x; \alpha) = \{y \in \mathcal{Y} : l(x, y) \leq \hat{Q}(\alpha)\}.$$

See Angelopoulos and Bates (2021) for a comprehensive survey of CP.

Figure 2 Overall architecture of the CREDO framework.



Note. The two main steps are: (i) Map the given candidate decision z (e.g., $(0, 0)$) to its inverse feasible region $\pi^{-1}(z)$; (ii) Assess the risk by constructing prediction sets within $\pi^{-1}(z)$ using generative conformal prediction, and extracting their miscoverage levels.

4.2. Conformalized Decision Risk Assessment

We now develop our framework for estimating the decision risk $\alpha(z)$ defined in Section 3. We accomplish this by reformulating the optimality probability in (2) as an *inverse* CP problem, where we seek to quantify how often uncertain parameters fall within regions that render a decision optimal. The key idea is to project the decision's optimality condition onto an *inverse feasible region* (Chan et al. 2025, Tavashioğlu et al. 2018) in the space of \mathcal{Y} , and to construct inner geometric approximations of this region using multiple generated conformal balls (Shafer and Vovk 2008, Wang et al. 2023). The resulting average miscoverage rate across balls then serves as a data-driven lower-bound of decision risk. We detail this procedure in two steps, illustrated in Figure 2.

4.2.1. Reformulation with Inverse Feasible Region Our first step reformulates (2) as an inverse optimization problem. For any given realization y , a decision z is (near-)optimal if and only if it attains the (near-)minimal objective value among all feasible decisions. Accordingly, we define *inverse feasible region* as the set of scenarios y under which z remains the (near-)optimal decision. Formally,

$$\pi_{\epsilon}^{-1}(z) := \left\{ y \in \mathcal{Y} \mid f(z; y) \leq \min_{z' \in \mathcal{Z}} f(z'; y) + \epsilon \right\}. \quad (4)$$

This definition generalizes its classical notion defined by Chan et al. (2025), providing a relaxed definition that accommodates near-optimal decisions. In parallel with our notation for π , we use π^{-1} to denote π_ϵ^{-1} except where the distinction matters.

LEMMA 1 (Reformulation). *The probability in (2) can be equivalently expressed as:*

$$\mathbb{P}\{z \in \pi(Y)\} \equiv \mathbb{P}\{Y \in \pi^{-1}(z)\}. \quad (5)$$

Its proof follows immediately by the definition of $\pi(Y)$ and $\pi^{-1}(z)$. This equivalence has important computational implications: the original formulation in (2) requires computing the probability that a fixed decision z lies in the random (near-)optimal set $\pi(Y)$. This task remains computationally intractable because it entails solving the underlying optimization problem for every possible realization of Y . By contrast, the reformulation in Lemma 1 reverses this viewpoint by evaluating the probability that the *random* variable Y lies within the *deterministic* region $\pi^{-1}(z)$. This shift yields a tractable probability estimation problem.

4.2.2. Risk Estimation via Generative Conformal Prediction The second step estimates the probability $\mathbb{P}\{Y \in \pi^{-1}(z)\}$. Direct estimation is generally intractable, as it requires computing the probability mass over $\pi^{-1}(z)$ —a region with complex and implicitly defined geometry. Such estimation typically demands either strong parametric assumptions on the distribution of Y or efficient sampling access to it, neither of which is often feasible in practice. A common workaround is to train a conditional generative model that samples from $\mathcal{P}_{Y|X}$ and then approximate the desired probability by the fraction of these samples falling within $\pi^{-1}(z)$. However, this approach lacks any finite-sample guarantee for the validity requirement in (2).

To address this, we develop a generative conformal approach that constructs statistically valid inner approximations of $\pi^{-1}(z)$ using calibration data. Given an input X , we generate a collection of CP balls $C(X; \alpha)$ such that (i) each region lies entirely within $\pi^{-1}(z)$ and (ii) its coverage probability

is lower-bounded with statistical guarantees obtained from calibration. This yields the following bound on decision risk:

$$\mathbb{P}\{Y \in \pi^{-1}(z)\} \stackrel{(i)}{\geq} \mathbb{P}\{Y \in C(X; \alpha)\} \stackrel{(ii)}{\geq} 1 - \alpha. \quad (6)$$

The right-hand guarantee follows from the finite-sample validity of CP. To satisfy the left-hand inequality, we identify the smallest α for which the corresponding ball $C(X; \alpha)$ remains entirely within $\pi^{-1}(z)$. The resulting average value of α across generated balls provides a data-driven estimator of the decision risk, denoted by $\hat{\alpha}(z)$.

4.2.3. Proposed Algorithm We begin with training a (conditional) generative model $g : X \rightarrow \mathcal{Y}$ on a training dataset to approximate the conditional distribution $\mathcal{P}_{Y|X}$. Then, for a test input x , we draw a prediction $\hat{y} \sim g(x)$ and construct a prediction set as an ℓ_2 ball centered at \hat{y} :

$$C(x; \alpha) = \{y \in \mathcal{Y} \mid \|y - \hat{y}\|_2 < R(\alpha)\}, \quad (7)$$

where the radius $R(\alpha)$ is obtained by calibrating the non-conformity scores $\{L_i\}_{i=1}^n$ on \mathcal{D} . Of note, smaller α corresponds to larger $R(\alpha)$ and higher empirical coverage. We consider three specifications of the radius function $R(\alpha) : [0, 1] \rightarrow \mathbb{R}_+ \cup \{\infty\}$, each satisfying the boundary conditions $R(\alpha) = \infty$ for $\alpha \in [0, 1/(n+1))$ and $R(1) = 0$. For $\alpha \in [1/(n+1), 1)$, we specify:

$$R_p(\alpha) = \hat{Q}(\alpha); \quad (p\text{-value radius}) \quad (8)$$

$$R_e(\alpha) = \frac{\sum_{i=1}^n L_i}{\alpha(n+1) - 1}; \quad (e\text{-value radius}) \quad (9)$$

$$R_\infty(\alpha) = \infty, \quad (\text{Monte Carlo radius}) \quad (10)$$

for $\alpha \in [1/(n+1), 1)$, where $\mathbb{1}\{\cdot\}$ is the indicator function. Here, R_p corresponds to the classical conformal radius based on the empirical quantiles of calibration residuals (Vovk et al. 2005, Singh et al. 2024); R_e is an e -value-based variant (Grünwald et al. 2024), offering stronger post-hoc

validity guarantees (Vovk 2025, Balinsky and Balinsky 2024, Gauthier et al. 2025b); and R_∞ is used in a Monte Carlo-based estimation. We will later discuss their respective validity properties, showing that R_e provides the strongest robustness, R_∞ the highest accuracy, and R_p a balanced trade-off between the two.

For all variants, the coverage level of each generated prediction set is determined by solving

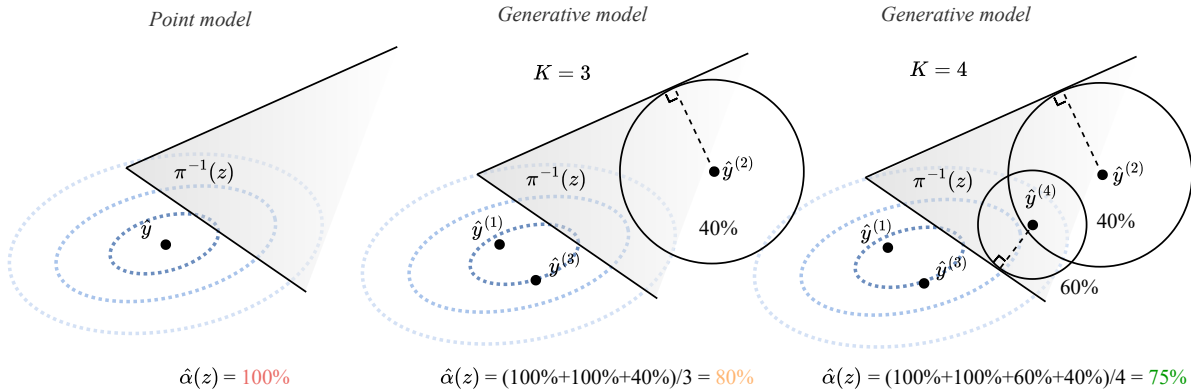
$$\tilde{\alpha}(z) = \min_{\alpha \in [0,1]} \alpha \quad \text{s.t.} \quad C(x; \alpha) \subseteq \pi^{-1}(z). \quad (11)$$

The entire procedure above is repeated across K sets to obtain the collection of estimates $\{\tilde{\alpha}^{(k)}(z)\}_{k=1}^K$, which are then averaged to yield the final risk estimator:

$$\hat{\alpha}(z) = \left(\tilde{\alpha}^{(1)}(z) + \dots + \tilde{\alpha}^{(K)}(z) \right) / K. \quad (12)$$

We highlight the necessity of using generative models in estimating (12) by contrasting them with traditional point prediction models commonly used in standard CP. As illustrated in Figure 3, point prediction models may produce outputs that lie near the boundary of, or even outside, the inverse feasible region $\pi^{-1}(z)$, leading to overly conservative risk estimates (*i.e.*, extremely small or even

Figure 3 Comparative illustration of risk estimation using a point model and generative models ($K = 3$ and $K = 4$) in CREDO.



Note. The gray shaded area represents the inverse feasible region $\pi^{-1}(z)$. The blue dotted ellipsoids represent the conditional distribution of $Y|X$, and the black dots indicate model predictions $\hat{y}^{(k)}$. The balls indicate calibrated prediction sets $C^{(k)}(x; \hat{\alpha}(z))$.

Algorithm 1 Conformalized Decision Risk Assessment (CREDO)

Require: Fitted generative model g ; Calibration dataset $\{(x_i, y_i)\}_{i=1}^n$; Sample size K ; Decision z ;

Test covariate x ;

- 1: Initialize nonconformity score set $\mathcal{L} \leftarrow \emptyset$;
 - 2: **for** $i \in \{1, \dots, n\}$ **do**
 - 3: $\hat{y}_i \sim g(x_i)$; $L_i \leftarrow \|y_i - \hat{y}_i\|_2$; $\mathcal{L} \leftarrow \mathcal{L} \cup \{L_i\}$;
 - 4: **end for**
 - 5: **for** $k = 1, \dots, K$ **do**
 - 6: $\hat{y}^{(k)} \sim g(x)$ generate prediction using x ;
 - 7: $C^{(k)}(x; \alpha) \leftarrow$ construct conformal set given \mathcal{L} and $\hat{y}^{(k)}$ via (7);
 - 8: $\tilde{\alpha}^{(k)}(z) \leftarrow$ solve for the k -th decision risk via (11);
 - 9: **end for**
 - 10: $\hat{\alpha}(z) \leftarrow 1/K \cdot \sum_{k=1}^K \tilde{\alpha}^{(k)}(z)$.
 - 11: **return** Risk estimator $\hat{\alpha}(z)$.
-

zero values when predictions fall outside the region). In contrast, generative models enable multiple stochastic draws; increasing K improves the likelihood that at least one sample lies within $\pi^{-1}(z)$, yielding more accurate and less conservative risk estimates. This insight will later be formalized through the notion of the true positive rate in our theoretical analysis. The complete algorithmic procedure is summarized in Algorithm 1.

5. Theoretical Analysis

In this section, we now establish the statistical properties of our risk estimator $\hat{\alpha}(z)$, providing three main theoretical results. First, we show that our estimator is “conservative” (Theorem 1), ensuring it provides a valid upper bound on the true decision risk. Second, we prove that the estimator is asymptotically consistent (Proposition 1), admitting a tight characterization for the decision risk in

large samples. Finally, we highlight the pivotal role of the generative model in our framework by analyzing the estimator’s true positive rate (Proposition 2), which directly influences the quality of downstream decisions. All proofs are deferred to Appendix A.

5.1. Validity

A fundamental requirement for any risk assessment tool is that it provides reliable guarantees. We therefore first establish that CREDO’s risk estimates are conservative for both the e - and p -value radii, ensuring practitioners can trust the bounds provided by our framework.

THEOREM 1 (Conservativeness under e -value). *Under Assumption 1 and $R(\alpha) = R_e(\alpha)$, the estimator $\hat{\alpha}(z)$ in (12) satisfies*

$$\mathbb{P}\{z \in \pi(Y)\} \geq 1 - \mathbb{E}[\hat{\alpha}(z)].$$

Thus, $\hat{\alpha}(z)$ provides an expectation-wise upper bound on the true decision risk, without requiring correctness of the generative model. This highlights the robustness of the e -value construction. We now examine the corresponding guarantee for the p -value radius.

COROLLARY 1 (Conservativeness under p -value). *Under Assumption 1 and $R(\alpha) = R_p(\alpha)$,*

$$\mathbb{P}\{z \in \pi(Y)\} \geq 1 - \mathbb{E}[\hat{\alpha}(z)] - \frac{1}{n+1} \sum_{i=1}^n d_{\text{TV}}^{(i)}(\hat{\alpha}(z)),$$

where $d_{\text{TV}}^{(i)}(\hat{\alpha}(z))$ is the conditional total variation (TV) distance between the data vector and the same vector with entries i and $(n+1)$ swapped.

The additional TV term reflects the deviation from full exchangeability caused by post-hoc selection of $\hat{\alpha}(z)$ (Barber et al. 2023, Gauthier et al. 2025a). While R_e enjoys exact conservativeness, we later show that R_p offers improved empirical tightness (or accuracy).

5.2. Consistency

We next study whether $\hat{\alpha}(z)$ converges to the true risk under mild assumptions on the generative model, measured through total variation distance $d_{TV}(\cdot, \cdot)$.

PROPOSITION 1 (Asymptotic conditional consistency). *Let $\hat{\mathcal{P}}_{Y|X}$ be the conditional distribution learned by the generative model g . If for some $\delta \geq 0$,*

$$d_{TV}(\hat{\mathcal{P}}_{Y|X=x}, \mathcal{P}_{Y|X=x}) \leq \delta \quad \text{for all } x \in \mathcal{X},$$

then with $R(\alpha) = R_\infty(\alpha)$, the estimator (12) satisfies

$$|\hat{\alpha}(z) - \mathbb{P}\{z \notin \pi(Y) \mid X = x\}| \leq O_p(K^{-1/2}) + \delta.$$

Proposition 1 guarantees marginal consistency as $K \rightarrow \infty$, provided that the generative model approximates the conditional distribution within TV distance δ . Thus, with a well-trained model and sufficiently many generated samples, $\hat{\alpha}(z)$ converges at a parametric rate to the true decision risk, complementing the finite-sample conservativeness of Theorem 1.

5.3. True Positive Rate

We conclude by analyzing how often the estimator correctly retains feasible decisions. Define the true positive rate as

$$\text{TPR}(K) := \frac{\mathbb{E} \left[\#\{z \in \mathcal{Z} : \alpha(z) < 1 \text{ and } \sum_{k=1}^K \tilde{\alpha}^{(k)}(z) < 1\} \right]}{\#\{z \in \mathcal{Z} : \alpha(z) < 1\}}, \quad (13)$$

where $\alpha(z) = \mathbb{P}\{z \notin \pi(Y)\}$ is the true risk. TPR measures the fraction of genuinely feasible decisions that are not mistakenly discarded by the estimator. From a practical perspective, TPR quantifies the ability of CREDO to correctly identify decisions that have non-trivial optimality probability while maintaining conservative guarantees. A low TPR corresponds to more “false-positive” exclusions, which may eliminate profitable or optimal decisions; thus, a higher TPR indicates better decision quality.

PROPOSITION 2 (True positive rate). *The $\text{TPR}(K)$ increases monotonically with K .*

Proposition 2 highlights the importance of using generative models and of sampling diversity: small K (e.g., $K = 1$) or deterministic predictors increase the likelihood of false exclusions, lowering TPR. Increasing K mitigates this issue and improves downstream decision quality. The result holds uniformly across all calibrated radii $R(\alpha)$.

Together, these results demonstrate that CREDO provides conservative risk estimates (validity), converges to the true risk under reasonable conditions (consistency), and benefits from generative sampling to avoid excessive conservatism (high TPR). These properties ensure both theoretical rigor and practical utility in decision support applications.

6. Computational Implementation

The theoretical analysis in the previous section establishes that CREDO provides conservative risk estimates with strong finite-sample guarantees. However, realizing these guarantees in practice requires efficiently evaluating (11) for each decision z and generated sample \hat{y} . This evaluation presents a fundamental computational challenge as we must verify whether a calibrated conformal ball $C(x; \alpha)$ is entirely contained within the inverse feasible region $\pi^{-1}(z)$. This is a set containment problem that is NP-hard in general.

This section develops practical algorithms to address this challenge. We begin by reformulating the geometric containment constraint into a tractable optimization problem (Section 6.1). Subsequently, we present efficient solution strategies for two important problem classes: linear programs, where we derive closed-form expressions, and general convex problems, where we employ gradient-based approximations (Section 6.2). These computational tools enable practitioners to deploy CREDO for real-world decision support while maintaining the theoretical guarantees established in Section 5.

6.1. Set-Containment Constraint Reformulation

We begin by noticing that the set containment condition $C(x; \alpha) \subseteq \pi^{-1}(z)$ is equivalent to requiring that the calibrated conformal ball does *not* intersect the complement of the inverse feasible region:

$$C(x; \alpha) \subseteq \pi^{-1}(z) \iff C(x; \alpha) \cap (\pi^{-1}(z))^c = \emptyset.$$

Since $C(x; \alpha)$ is an ℓ_2 ball centered at \hat{y} , the right hand side is further equivalent to

$$\underbrace{\text{for all } y \in (\pi^{-1}(z))^c, \|y - \hat{y}\|_2 \geq R(\alpha)}_{(i)} \quad \text{if } \underbrace{\hat{y} \in \pi^{-1}(z)}_{(ii)}.$$

Here, condition (i) requires that every scenario y violating the optimality of decision z must lie at least with distance $R(\alpha)$ away from \hat{y} ; condition (ii) states that the former condition is enforced only when \hat{y} lies within of $\pi^{-1}(z)$. Otherwise, then no radius can guarantee containment, and the α is trivially mapped to one by design. This reformulation allows us to circumvent the need for validating the original set containment relation defined in Equation (11), and derive a more principled computational representation, summarized as follows.

PROPOSITION 3 (Computational Reformulation). *Let \hat{y} be a generated prediction and $\tilde{\alpha}$ be its estimated risk. Then*

$$\tilde{\alpha}(z) = 1, \quad \text{if } z \notin \pi(\hat{y}), \quad (14a)$$

$$\tilde{\alpha}(z) = \sup_{y \in \mathcal{Y}} R^{-1}(\|y - \hat{y}\|_2) \quad \text{s.t.} \quad f(z; y) > \min_{z' \in \mathcal{Z}} f(z'; y) + \epsilon, \quad \text{if } z \in \pi(\hat{y}). \quad (14b)$$

where $R^{-1} : [0, \infty) \rightarrow [0, 1]$ is the inverse radius function:

$$R^{-1}(l) = \min_{\alpha \in [0, 1]} \{\alpha : R(\alpha) \leq l\}.$$

The inverse functions for the three calibrated radii in Equations (8)–(10) admit closed-form expressions, which makes the evaluation of the optimization problem explicit.

LEMMA 2. For the radii defined in Equations (8)–(10), the corresponding inverse functions are:

$$R_p^{-1}(l) = \left(1 - \frac{1}{n+1} \left[\sum_{i=1}^n \mathbb{1}\{L_i \leq l\} \right] \right)^+, \quad (15)$$

$$R_e^{-1}(l) = \left(\frac{\sum_{i=1}^n L_i + l}{(n+1)l} \right)^+, \quad (16)$$

$$R_\infty^{-1}(l) = 0, \quad (17)$$

where $(\cdot)^+ = \max\{0, \cdot\}$ denotes the rectified linear unit (ReLU) operator.

REMARK 1. Combining Equation (17) with Proposition 3, one can verify that the risk estimate computed with the Monte Carlo radius degenerates to the form:

$$\hat{\alpha}(z) = \frac{1}{K} \sum_{k=1}^K \mathbb{1}\{z \notin \pi(\hat{y}^{(k)})\}.$$

Namely, the risk estimator is essentially a Monte Carlo estimator of whether the generated samples from the generative model $f(x)$ fall inside $\pi(\hat{y}^{(k)})$.

6.2. Computational Strategies for Specific Problem Classes

Leveraging Proposition 3, the computation of each individual risk estimate $\tilde{\alpha}(z)$ proceeds in two stages: (i) Given a generated sample \hat{y} , we solve the optimization (1) once to check whether $z \in \pi(\hat{y})$. If this condition fails, we immediately set $\tilde{\alpha}(z) = 1$. Otherwise, we find $\tilde{\alpha}(z)$ via solving the optimization problem (14b). However, although optimization problem (14b) circumvents checking for set-containment, it may nonetheless remain NP-hard depending on the form of the objective $f(z; y)$ and the geometry of \mathcal{Z} . In what follows, we analyze computational strategies for specific problem classes: we first provide a closed-form estimator for the linear case, and then introduce a practical heuristic applicable to general convex decision models.

6.2.1. Linear Problems We first examine the special case in which the decision problem is a linear program of the form

$$f(z; y) := \langle y, z \rangle \quad \text{s.t.} \quad Az \leq b, \quad (18)$$

where $A \in \mathbb{R}^{m \times d}$ and $b \in \mathbb{R}^m$ define a nonempty polyhedral feasible region. Let \mathcal{V} denote the set of extreme points of this polytope, which can be solved from A and b using procedures such as the double description method (Motzkin et al. 1953, Fukuda and Prodon 1995).

In this setting, we can derive a closed-form solution for the optimization problem (14b) by leveraging \mathcal{V} , utilizing the property that the optimal solution to a linear program always occurs at an extreme point (Bertsimas and Tsitsiklis 1997). Specifically, by the linearity of $f(z; y)$, the constraint $f(z; y) > \min_{z' \in \mathcal{Z}} f(z'; y) + \epsilon$ is equivalent to requiring that for all extreme points¹ $v \in \mathcal{V} \setminus \{z\}$, there is $\langle y, z \rangle > \langle y, v \rangle + \epsilon$, which can be rearranged as a linear inequality $\langle y, z - v \rangle > \epsilon$. Consequently, its feasible region is the union of a finite number of halfspaces, each associated with a direction vector $z - v$ for $v \in \mathcal{V} \setminus \{z\}$. Therefore, the original optimization problem (14b) reduces to evaluating a finite set of closed-form expressions, yielding an explicit formula for the risk estimate.

PROPOSITION 4 (Closed-Form Risk for Linear Programs). *Under (18), the risk estimate $\tilde{\alpha}(z)$ for a single generated sample \hat{y} admits the closed-form expression:*

$$\tilde{\alpha}(z) = \max_{v \in \mathcal{V} \setminus \{z\}} R^{-1} \left(\frac{|\langle \hat{y}, z - v \rangle - \epsilon|}{\|z - v\|_2} \right), \quad \text{if } z \in \pi(\hat{y}).$$

6.2.2. Convex Problems In the linear setting, the success in deriving a closed-form estimate critically relies on the polyhedral description of the ϵ -suboptimality region. However, for general convex decision problems, where we assume \mathcal{Z} is convex and $f(z; y)$ is convex in each argument marginally, such a representation is unavailable. Additionally, this also renders the constraint $f(z; y) - \min_{z' \in \mathcal{Z}} f(z'; y) > \epsilon$ to be potentially nonconvex in (z, y) , and cannot be directly handled by off-the-shelf convex solvers.

We adopt a heuristic algorithm (Algorithm 2) that combines ideas from the difference-of-convex algorithm (DCA) (Tao and An 1997) and coordinate descent (Wright 2015) to solve for

¹ Excluding z because it never satisfies the constraint with $\epsilon \geq 0$.

Problem (14b). By the monotonically decreasing property of $R^{-1}(\cdot)$, we begin by noticing that the original optimization problem can be reformulated as first solving the following single-level minimization problem²

$$\min_{y, z'} \|y - \hat{y}\|_2 \quad \text{s.t.} \quad f(z; y) - f(z'; y) > \epsilon \quad \text{and} \quad z' \in \mathcal{Z}. \quad (19)$$

and then applying the inverse radius function $R^{-1}(\cdot)$ to the optimal objective value. To solve (19), which jointly minimizes over (y, z') , we adopt an alternating scheme that iteratively fixes one variable and solves the resulting marginal convex subproblem in the other. The algorithm starts by initialize y at the generated prediction $y^{(0)} = \hat{y}$. For each iteration $t = 1, \dots, T$, the procedure: (i) Solve for $z^{(t)}$, which is computed as the optimal solution to the original decision-making problem with $y = y^{(t-1)}$. It represents the most feasible solution $z \in \mathcal{Z}$ at the current iteration, as one can verify that it maximizes the slack of the constraint in Problem (19). (ii) Solve for $y^{(t)}$, where we adopt a convex surrogate to the original constraint by approximating $f(z; y)$ with its first-order Taylor expansion, which can then be solved with standard solvers. After T iterations, the final iterate $y^{(T)}$ is used to form the approximate risk estimate

$$\tilde{\alpha}(z) := R^{-1} \left(\|y^{(T)} - \hat{y}\|_2 \right), \quad \text{if } z \in \pi(\hat{y}).$$

In our experiments, we empirically validate this adopted approach by showing it is reliable for producing high-quality risk estimates, providing a computationally tractable solution to decision risk assessment tasks in broader convex settings.

7. Experiments

In this section, we evaluate the performance of CREDO through extensive numerical experiments. Our results demonstrate that: (i) High-quality risk estimation (Section 7.1). CREDO produces

² Without loss of generality, we assume \mathcal{Y} to be the whole space.

Algorithm 2 Alternating Optimization for Solving (14b) in General Convex Settings

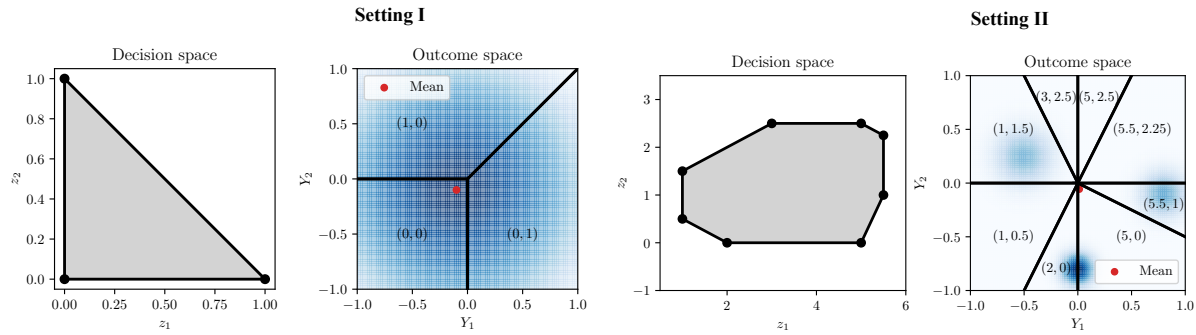
Require: Prediction \hat{y} ; Decision z ; Tolerance level ϵ .

```

1:  $y^{(0)} \leftarrow \hat{y}$  initialization;
2: for  $t \in \{1, \dots, T\}$  do
3:    $z^{(t)} \leftarrow \arg \min_{z' \in \mathcal{Z}} f(z'; y^{(t-1)})$ .
4:    $\tilde{f}^{(t)}(z; y) \leftarrow f(z; y^{(t-1)}) + \left\langle \nabla_y f(z; y) \Big|_{y=y^{(t-1)}}, y - y^{(t-1)} \right\rangle$ .
5:    $y^{(t)} \leftarrow \arg \min_{y \in \mathcal{Y}} \|y - \hat{y}\|_2 \quad \text{s.t.} \quad \tilde{f}^{(t)}(z; y) - f(z^{(t)}; y) > \epsilon$ 
6: end for
7: return  $R^{-1}(\|y^{(T)} - \hat{y}\|_2)$ .
```

risk estimates that can be tuned toward either conservativeness or accuracy through the choice of radius, with both aspects outperforming baseline models. This flexibility underscores its suitability for decision risk-assessment tasks. *(ii)* Risk-aware decision prescriptions (Section 7.2). The risk estimates produced by CREDO can be directly used to prescribe decisions that achieve consistent low risk, demonstrating CREDO’s reliability as a practical tool for risk-aware decision making. *(iii)* Effective modular design (Section 7.3). Each component of CREDO exhibits superior performance on its respective subtask compared with alternative ablation variants, highlighting the advantages of our modeling choices.

Our experiments span a variety of optimization structures, including linear programming (LP), quadratic programming (QP), second-order conic programming (SOCP), integer programming (IP), and a penalized knapsack problem that uses semi-synthetic data from a real-world grid infrastructure investment problem (Real Data). Specifically, LP includes two stylized settings referred to as Setting I and Setting II, shown in Figure 4. Setting I features a triangular feasible region with three vertices, with a highly stochastic distribution of Y . Setting II represents a more complex scenario with an octagonal feasible region comprising five vertices, with a more dispersed and multimodal

Figure 4 Illustration of settings I and II.

Note. The gray region represents the feasible region in the decision space, and the cones to the right are the corresponding inverse feasible regions in the outcome space. The blue shade denotes the density mass of Y .

distribution of Y . These two settings are consistently used throughout the experiments due to their high interpretability and simplicity. The variance of the synthetic data distribution is controlled by a σ parameter, which is specified by the user. Additional details of optimizations are provided in Section B.

7.1. Risk Estimation Evaluation

In this subsection, we evaluate CREDO's ability to produce risk estimates that flexibly trade off conservativeness and accuracy depending on the choice of radius, demonstrating that it outperforms baseline models along both dimensions. To this end, we benchmark CREDO's risk estimation performance against generic probability estimation baselines. Note that the quantity of interest, $\mathbb{P}\{z \in \pi(Y)\}$, can be interpreted as predicting, for a given test instance (x, y) , the probability that a prescribed decision remains ϵ -optimal under y . This perspective naturally allows us to adapt standard regression and classification models as baselines for the decision risk-assessment task.

Specifically, we consider five representative baseline models: (i) SA: sample average of the historical data ϵ -optimality condition indicators; (ii) LR: logistic regression; (iii) NN: a neural network-based (multi-layer perceptron) classifier; (iv) QR: quantile regression model; (v) CP: conformal prediction model using the upper prediction interval as its output. These baseline models capture the types of prediction approaches that decision-makers are likely to adopt as main candidates

Table 1 Evaluated metrics for different risk estimation methods across different optimization settings.

	LP Setting I		LP Setting II		QP ($\epsilon = 0.1$)		SOCP ($\epsilon = 0.2$)		IP ($\epsilon = 0.3$)	
	Validity (\uparrow)	MAE (\downarrow)	Validity (\uparrow)	MAE (\downarrow)	Validity (\uparrow)	MAE (\downarrow)	Validity (\uparrow)	MAE (\downarrow)	Validity (\uparrow)	MAE (\downarrow)
SA	0.53 ± 0.50	0.04 ± 0.03	0.56 ± 0.44	0.03 ± 0.02	0.43 ± 0.48	0.04 ± 0.03	0.47 ± 0.48	0.03 ± 0.03	0.41 ± 0.46	0.04 ± 0.03
LR	0.50 ± 0.48	0.06 ± 0.04	0.59 ± 0.39	0.03 ± 0.02	0.47 ± 0.50	0.05 ± 0.04	0.50 ± 0.45	0.06 ± 0.05	0.45 ± 0.46	0.07 ± 0.04
NN	0.50 ± 0.45	0.10 ± 0.09	0.39 ± 0.38	0.05 ± 0.03	0.63 ± 0.46	0.08 ± 0.05	0.40 ± 0.48	0.08 ± 0.06	0.48 ± 0.49	0.09 ± 0.06
QR	0.00 ± 0.00	0.62 ± 0.13	0.89 ± 0.16	0.15 ± 0.06	0.03 ± 0.10	0.60 ± 0.10	0.00 ± 0.00	0.56 ± 0.00	0.14 ± 0.04	0.53 ± 0.06
CP	1.00 ± 0.00	0.31 ± 0.00	1.00 ± 0.00	0.12 ± 0.00	1.00 ± 0.00	0.37 ± 0.00	1.00 ± 0.00	0.43 ± 0.01	1.00 ± 0.00	0.31 ± 0.00
CREDO (p)	1.00 ± 0.00	0.27 ± 0.01	1.00 ± 0.00	0.11 ± 0.00	1.00 ± 0.00	0.16 ± 0.03	1.00 ± 0.00	0.38 ± 0.02	1.00 ± 0.00	0.25 ± 0.02
CREDO (e)	1.00 ± 0.00	0.31 ± 0.00	1.00 ± 0.00	0.12 ± 0.00	1.00 ± 0.00	0.18 ± 0.04	1.00 ± 0.00	0.44 ± 0.00	1.00 ± 0.00	0.31 ± 0.00
CREDO (∞)	0.50 ± 0.50	<u>0.05 ± 0.03</u>	0.53 ± 0.43	<u>0.03 ± 0.02</u>	0.60 ± 0.48	<u>0.05 ± 0.03</u>	0.53 ± 0.49	<u>0.05 ± 0.03</u>	0.47 ± 0.47	<u>0.05 ± 0.04</u>

for estimating decision risk. We adopt two evaluation metrics for the decision risk estimate: (i) Validity: the ratio of trials where the estimated risk successfully upper bounds the true risk; (ii) MAE: the mean absolute error of the risk estimate compared to the true risk. These two metrics represent quantifies conservativeness and accuracy, which are the two crucial dimensions of risk estimate evaluation. Additional details of the experimental settings are included in Section B.

Table 1 summarizes the results³. For the first three baselines (SA, LR, NN), we observe low estimation error but poor validity. This is expected: these models are trained to maximize predictive accuracy, not conservativeness, and thus systematically underestimate risk. In contrast, the last two baselines (QR and CP) exhibit higher validity but substantially larger errors. Although both approaches can enforce conservativeness by adjusting the quantile level q , the choice of q is continuous in $[0, 1]$ and lacks any principled mechanism to guarantee validity across problems or distributional shifts. By comparison, CREDO achieves the best of both worlds. With p -value and e -value radii, CREDO attains 100% validity across all settings; with the Monte Carlo radius, it yields highly accurate risk estimates with (near) minimal error. Together, these results highlight the versatility of CREDO: it can be tuned to deliver either guaranteed conservativeness or high-precision estimation, offering a principled and robust framework for decision risk assessment.

³ Results are reported as mean \pm standard deviation across trials. Boldface indicates the best result, and underlining indicates the second best within the same setting. This convention applies to all tables in the experiment.

7.2. Decision Prescription Evaluation

In this part, we examine CREDO’s performance when its outputted risk estimate is combined with the risk minimization criterion to prescribe decisions, where the candidate decision with the lowest risk is selected as the output. we show that CREDO can be used to select decisions with consistently high confidence, demonstrating its effectiveness in guiding practical decision-making.

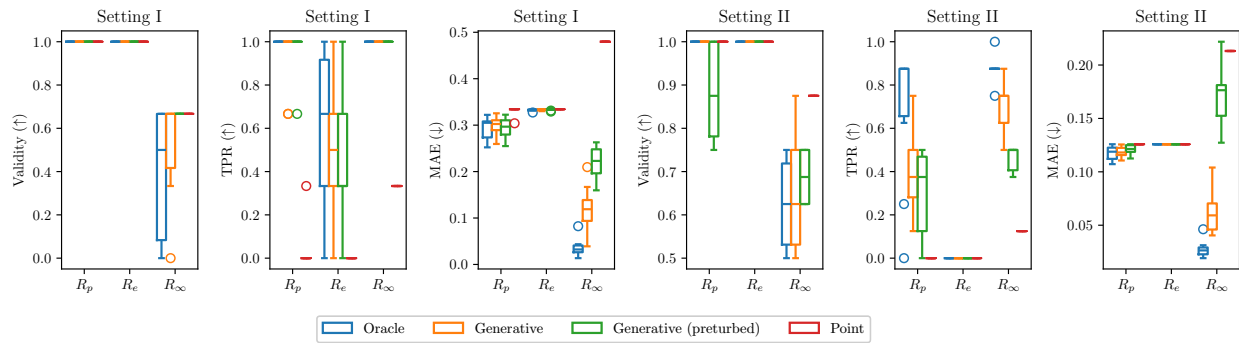
We benchmark CREDO against four baselines: predict-then-optimize (PTO) (Bertsimas and Kallus 2020), robust optimization (RO) (Bertsimas and Thiele 2006), smart predict-then-optimize (SPO+) (Elmachtoub and Grigas 2022), and decision-focused learning (DFL) (Amos and Kolter 2017). These methods are chosen for comparison as they represent widely used, risk-averse, data-driven approaches. For CREDO’s generative model design, we adopt four different variants: the Gaussian Mixture model (GMM) with one, three, and five components, as well as the variational autoencoder (VAE) (Kingma and Welling 2013). We use *empirical confidence ranking* as our primary evaluation metric: given a decision policy π and a test dataset $\{(x_i, y_i)\}_{i=1}^m$, we apply π to each input x_i to generate predicted decisions $\{z_i\}_{i=1}^m$. We then compute the score $\sum_{i=1}^m \phi(z_i)$, where $\phi : \mathcal{Z} \rightarrow \mathbb{Z}_+$ is a mapping that maps each prediction to a discrete rank based on its frequency among the ground-truth optimal decisions $\{z_i^*\}_{i=1}^m$ in the test set. This metric is designed to capture a method’s tendency to select decisions that are most likely to be optimal—a direct representation of risk in decision-making contexts.

Table 2 presents the comparison results. It can be seen that CREDO achieves the smallest ranking metric value across most datasets, on average selecting the top two most likely decisions across all datasets. Though it might seem concerning that the in Setting I ($\sigma = 0.1$), PTO, RO, and SPO+ all achieve better performance than CREDO, this is because when σ is small, the data becomes highly concentrated around the mean, rendering the problem nearly deterministic and can be best dealt with point-prediction baselines. Across different generative model designs in CREDO, the

Table 2 Evaluated empirical confidence ranking (\downarrow) for different methods across three datasets.

Method	Setting I			Setting II			Real Data
	$\sigma = 0.1$	$\sigma = 1$	$\sigma = 10$	$\sigma = 0.1$	$\sigma = 1$	$\sigma = 10$	
PTO	1.00 ± 0.00	2.76 ± 0.59	2.24 ± 0.79	3.55 ± 0.50	<u>3.36 ± 0.48</u>	2.04 ± 1.65	<u>1.75 ± 1.69</u>
RO	1.00 ± 0.00	2.98 ± 0.14	3.00 ± 0.00	4.99 ± 0.10	6.00 ± 0.00	3.98 ± 0.80	3.00 ± 1.29
SPO+	1.00 ± 0.00	2.68 ± 0.65	2.02 ± 0.82	3.95 ± 1.20	4.67 ± 1.56	3.56 ± 1.50	2.67 ± 1.43
DFL	2.44 ± 0.64	1.83 ± 0.81	2.06 ± 0.79	3.60 ± 1.52	3.96 ± 2.07	3.66 ± 2.48	1.92 ± 1.04
CREDO (1-GMM)	1.94 ± 0.87	1.56 ± 0.54	<u>1.49 ± 0.50</u>	3.74 ± 0.98	3.94 ± 1.37	2.02 ± 1.41	1.92 ± 1.04
CREDO (3-GMM)	1.75 ± 0.77	1.61 ± 0.56	1.48 ± 0.52	1.05 ± 0.22	1.00 ± 0.00	2.03 ± 0.96	1.75 ± 0.92
CREDO (5-GMM)	1.89 ± 0.87	1.65 ± 0.62	1.54 ± 0.52	<u>1.03 ± 0.17</u>	1.00 ± 0.00	<u>1.92 ± 0.89</u>	1.92 ± 1.04
CREDO (VAE)	<u>1.01 ± 0.10</u>	<u>1.61 ± 0.58</u>	1.77 ± 0.71	1.00 ± 0.00	1.00 ± 0.00	1.06 ± 0.24	1.92 ± 1.04

Figure 5 Comparison of three different calibrated radii.

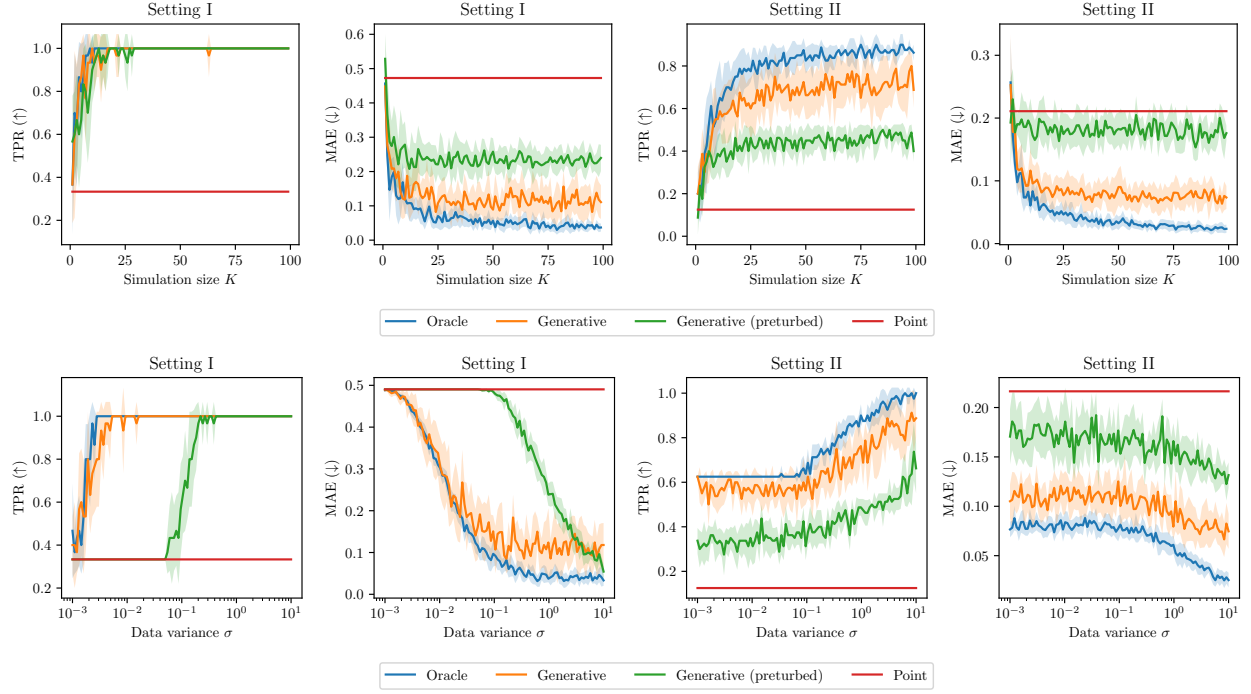


1-GMM performs significantly worse than the other generative model specifications. Among the remaining models, VAE and 5-GMM generally achieve slightly better performance than 3-GMM across most trials. This trend supports the intuition that more expressive generative models within CREOD lead to improved risk estimation, which further improves its capability to guide risk-aware decision making, especially under highly uncertain environments.

7.3. Ablation Studies

In this part, we examine ablation variants of CREDO through three controlled experiments that isolate the effects of radius design, generative modeling, and optimization procedures. These studies provide insight into CREDO’s sensitivity while also demonstrating the effectiveness of our design choices.

Figure 5 presents the evaluation results comparing different types of calibrated radii (R_p , R_e and R_∞) under different settings and generative model designs. It can be seen that both R_p and R_e

Figure 6 Comparison of four different configurations of the generative models.

Note. *Point* is constant across different specifications of K and σ , as they do not affect the fitting of the point prediction model.

achieve a 100% conservativeness rate across nearly all settings, while R_∞ only achieves around 50%. However, in terms of TPR and MAE, R_p attains substantially better performance than both R_e and R_∞ . This pattern was also observed in Section 7.1, and here we further dig deeper to analyze the underlying insights: (i) Although for R_p , a formal theoretical proof of conservativeness is not available, it empirically demonstrates comparably strong conservativeness as R_e . (ii) Even though R_∞ fails to ensure conservativeness, it achieves superior accuracy compared to both R_p and R_e by fully exploiting the generative model's fidelity. These insights highlight an essential trade-off when deploying CREDO: decision-makers must choose the calibrated radius according to their priorities. If conservativeness is paramount, R_p and R_e should be preferred; if accuracy is more critical, R_∞ is the better choice. Additionally, a consistent pattern can be observed from Figure 5: for both the TPR and accuracy metrics, R_p achieves substantially higher values than R_e across all settings. Since their conservativeness rates are nearly identical, this indicates that R_p may serve as a more practical and effective choice than R_e , despite lacking a formal theoretical guarantee.

Consequently, R_p can be interpreted as a balanced compromise between R_e and R_∞ , suitable for scenarios where conservativeness and accuracy are of comparable importance.

For the second set of ablation studies, we implement CREDO with four different configurations of the underlying prediction (generative) model: (i) *Oracle*: using the ground-truth data distribution as the generative model. (ii) *Generative*: a three-component Gaussian Mixture model, fitted using the EM algorithm for 1×10^2 epochs. (iii) *Generative (perturbed)*: same as *Generative* except that the fitted mean of the components is perturbed with a small noise, which follows a $U(0.5, 1)$ distribution. (iv) *Point*: point prediction model that captures the mean of the marginal distribution of Y . The metrics used in this experiment follow those in the risk-estimation evaluation (Section 7.1), with the addition of the true positive rate (TPR).

Figure 5 presents the evaluation results comparing different types of calibrated radii. We observe that R_p and R_e achieve a 100% conservativeness rate across nearly all settings, while R_∞ maintains only about 50%. However, in terms of TPR and accuracy, R_p attains substantially higher values than both R_e and R_∞ . Two key insights emerge: (i) Although we lack a formal theoretical proof of conservativeness for R_p as established for R_e in Theorem 1, R_p empirically demonstrates comparably strong empirical performance on conservativeness. (ii) Despite its failure to ensure conservativeness, R_∞ achieves superior accuracy, as it behaves as a Monte Carlo estimator that fully exploits the generative model’s fidelity. Overall, these findings highlight an essential trade-off when deploying CREDO: decision-makers must choose the calibrated radius according to their priorities. If conservativeness is paramount, R_e or R_p should be preferred; if accuracy is more critical, R_∞ is the better choice. Additionally, a consistent pattern can be observed from Figure 5: for both the TPR and accuracy metrics, R_p achieves substantially higher values than R_e across all settings. Since their conservativeness rates are nearly identical, this indicates that R_p may serve as a more practical and effective choice than R_e , despite lacking a formal theoretical guarantee.

Table 3 Evaluated metrics for different optimization procedures solving (14b) across different settings.

	LP Setting I			LP Setting II			QP			SOCP			IP		
	Obj	Vio	Err	Obj	Vio	Err	Obj	Vio	Err	Obj	Vio	Err	Obj	Vio	Err
GD	<u>0.44</u>	0.40	0.45	<u>0.06</u>	<u>0.07</u>	<u>0.05</u>	0.60	0.23	0.50	1.53	0.13	1.31	0.22	0.00	0.19
BF	0.66	0.00	<u>0.43</u>	0.11	0.00	0.10	<u>0.52</u>	0.00	<u>0.34</u>	<u>0.66</u>	0.00	<u>0.44</u>	<u>0.11</u>	0.00	<u>0.09</u>
RS	0.89	0.00	0.66	0.12	0.00	0.11	0.70	0.00	0.52	0.91	0.00	0.69	0.12	0.00	0.10
RG	5.21	<u>0.20</u>	4.98	1.35	0.17	1.34	4.81	0.17	4.63	5.21	0.17	4.99	1.35	0.00	1.32
CREDO	0.23	0.00	0.00	0.01	0.00	0.00	0.10	<u>0.10</u>	0.08	0.14	<u>0.03</u>	0.08	0.00	0.00	0.02

Consequently, R_p can be interpreted as a balanced compromise between R_e and R_∞ , suitable for scenarios where conservativeness and accuracy are of comparable importance.

Figure 6 presents the comparison results of CREDO risk estimation using different generative models. Across all settings, it can be observed that as both K and σ increase, the three generative-based methods (*Oracle*, *Generative*, and *Generative (perturbed)*) exhibit a clear improving trend, whereas the *Point* model remains constant. This pattern indicates that incorporating generative models within CREDO enhances the accuracy of risk estimation, particularly when the underlying data exhibit strong stochasticity (*i.e.*, larger variance). Moreover, the trends in Figure 6 generally follow the order $Oracle > Generative > Generative (perturbed) > Point$. Since both *Generative (perturbed)* and *Point* can be regarded as instances of misspecified models, this observation highlights that a well-trained generative model plays a crucial role in achieving accurate risk estimation.

In the last set of experiments, we evaluate the performance of different optimization procedures solving Problem (14b). We use three general metrics: (i) *Obj*: the solution's objective value averaged across trials; (ii) *Vio*: the average ratio of solutions that violate the optimization constraint. and (iii) *Err*: the average distance between the solution and the ground-truth solution. The ground truth solution is computed from the closed-form solution under the linear setting, and approximated using a highly granular brute-force enumeration strategy in nonlinear settings. We include five baselines: (i) GD: a generic gradient descent algorithm solving the optimization by penalizing the objective function with the constraint; (ii) BF: brute force enumeration, where its discretization resolution is

set to be the same as the number of iterations T for other methods; (iii) RS: random search algorithm, which is similar to BF except that the enumeration is done via sampling from a standard Gaussian distribution; (iv) RG: random guess, which is equivalent to a one-step RS. These baselines are chosen as they are to the best of our knowledge, the few tractable procedures that can effectively handle Problem (14b). To ensure fair comparison, all the above optimization baselines are tuned with the number of iterations and/or epochs such that they take approximately the same time to run as our proposed method.

Table 3 reports the comparison of optimization procedures. Across all settings, CREDO consistently achieves low error. In the linear setting, CREDO attains zero error because the corresponding closed-form estimator recovers the exact solution. For nonlinear convex settings, CREDO continues to exhibit low overall error, attributable to its ability to balance achieving a small objective value (Obj) while maintaining a low violation ratio (Vio). Together, these results demonstrate that CREDO's optimization procedure effectively handles both linear and nonlinear problems, supporting its efficacy and suitability for decision risk–assessment tasks and yielding the strong risk-estimation performance observed in Section 7.1.

8. Discussion and Conclusions

We introduced CREDO, a distribution-free framework for decision risk assessment that fundamentally shifts the paradigm from prescribing decisions to evaluating their reliability under uncertainty. By combining inverse optimization with conformal prediction, CREDO provides calibrated estimates of the probability that any candidate decision may be suboptimal, enabling practitioners to audit both human-proposed and algorithm-generated decisions with statistical guarantees.

Our theoretical analysis establishes that CREDO achieves conservative risk estimates, providing expectation-wise validity even under model misspecification. The framework's consistency properties ensure that these bounds tighten asymptotically as more data becomes available, while the true positive

rate analysis demonstrates that generative sampling effectively reduces excessive conservatism. These properties position CREDO as both theoretically rigorous and practically useful, addressing the long-standing challenge of quantifying decision stability without distributional assumptions.

The computational strategies we developed make these theoretical guarantees accessible in practice. For linear programs, our closed-form solution leverages the polytope structure to evaluate risk efficiently through vertex enumeration. For general convex problems, our gradient-based approach using differentiable optimization layers provides a practical approximation scheme. While computational complexity increases with problem scale and the number of generative samples, the modular design allows decision makers to balance computational cost against the desired level of risk assessment fidelity.

Our empirical evaluation reveals important trade-offs that emerge when deploying CREDO. The choice of calibrated radius fundamentally determines the balance between conservativeness and accuracy. The e-value approach offers rigorous post-hoc validity guarantees, but alternatives such as the p-value variant provide tighter risk estimates at the cost of weakened validity. Selecting an appropriate radius thus requires balancing the trade-off between validity and informativeness, ensuring that decision support remains both safe and actionable. This flexibility allows practitioners to select the variant that best matches their risk tolerance and application requirements. Moreover, our experiments demonstrate that CREDO's effectiveness scales with the quality of the underlying generative model. While validity is maintained even under misspecification, the informativeness of risk estimates depends critically on how well the generative model captures the true parameter distribution.

The framework's applicability extends to operational domains where parameter uncertainty significantly impacts decision quality. For example, for inventory management systems, CREDO can evaluate the robustness of reorder point policies and safety stock levels against demand variability

and lead time uncertainty, providing quantitative assessments of when established inventory rules may fail to minimize total costs. Rather than prescribing singular optimal solutions, our framework provides decision-makers with risk profiles that characterize solution stability across the parameter space, enabling more informed trade-offs between expected performance and robustness. This paradigm shift from deterministic optimization to risk-aware assessment is particularly valuable in regulated industries where decision justification and risk documentation are required, as CREDO's calibrated guarantees provide auditable evidence of decision quality under uncertainty.

Several limitations of the current framework suggest directions for future research. (i) Overconservativeness with high-dimensional \mathcal{Y} : CREDO's risk estimates become increasingly loose as the dimension of \mathcal{Y} grows due to the curse of dimensionality—conformal sets expand in volume with dimension even at fixed coverage. While this preserves validity, it can reduce practical usefulness in decision-making tasks with many uncertain components. Future work may explore more flexible prediction-set geometries to improve efficiency (Izbicki et al. 2022, Zheng and Zhu 2024). (ii) Lack of convergence guarantees for the alternating algorithm: Our alternating scheme in Algorithm 2 works well empirically for solving (19), but a formal convergence analysis remains open. The problem structure suggests potential for adapting contraction-type or block coordinate descent results, offering a promising avenue for theoretical study. (iii) Human-in-the-loop evaluation: Because CREDO is intended to support human–algorithm collaboration, controlled user studies are useful to examine how real-world practitioners interact with its conservative risk assessments and whether these assessments improve decision quality relative to purely algorithmic recommendations.

To conclude, CREDO represents a step toward more transparent and accountable decision support systems. As machine learning increasingly influences critical decisions across all industry and public policy domains, the ability to quantify decision risk becomes essential for responsible deployment. The framework's distribution-free guarantees are particularly valuable in high-stakes settings where

distributional assumptions are difficult to verify or where model misspecification could have severe consequences. By enabling algorithms to express uncertainty about their recommendations, CREDO facilitates a more nuanced collaboration between human expertise and machine intelligence, where each can contribute their respective strengths.

9. Acknowledgement

Wenbin Zhou and Shixiang Zhu acknowledge partial support from the 2024 Block Center Seed Fund at Carnegie Mellon University and the 2024 GenAI Fellows program offered by the Tepper School of Business, Center for Intelligent Business. Agni Orfanoudaki acknowledges support from the AI² Partnership Grant (from the UKRI and the AXA Insurance company), which facilitated this work.

References

- Agrawal A, Amos B, Barratt S, Boyd S, Diamond S, Kolter Z (2019) Differentiable convex optimization layers. *Advances in Neural Information Processing Systems*.
- Ahuja RK, Orlin JB (2001) Inverse optimization. *Operations research* 49(5):771–783.
- Ajay A, Du Y, Gupta A, Tenenbaum J, Jaakkola T, Agrawal P (2022) Is conditional generative modeling all you need for decision-making? *arXiv preprint arXiv:2211.15657*.
- Amos B, Kolter JZ (2017) Optnet: Differentiable optimization as a layer in neural networks. *International conference on machine learning*, 136–145 (PMLR).
- Angelopoulos AN, Bates S (2021) A gentle introduction to conformal prediction and distribution-free uncertainty quantification. *arXiv preprint arXiv:2107.07511*.
- Aswani A, Shen ZJ, Siddiq A (2018) Inverse optimization with noisy data. *Operations Research* 66(3):870–892.
- Balinsky AA, Balinsky AD (2024) Enhancing conformal prediction using e-test statistics. *The 13th Symposium on Conformal and Probabilistic Prediction with Applications*, 65–72 (PMLR).
- Barber RF, Candes EJ, Ramdas A, Tibshirani RJ (2023) Conformal prediction beyond exchangeability. *The Annals of Statistics* 51(2):816–845.
- Ben-Tal A, Nemirovski A (2002) Robust optimization—methodology and applications. *Mathematical programming* 92(3):453–480.

- Bertsimas D, Boussioux L, Cory-Wright R, Delarue A, Digalakis V, Jacquillat A, Kitane DL, Lukin G, Li M, Mingardi L, et al. (2021) From predictions to prescriptions: A data-driven response to covid-19. *Health care management science* 24:253–272.
- Bertsimas D, Gupta V, Kallus N (2018) Robust sample average approximation. *Mathematical Programming* 171(1):217–282.
- Bertsimas D, Kallus N (2020) From predictive to prescriptive analytics. *Management Science* 66(3):1025–1044.
- Bertsimas D, Sim M (2004) The price of robustness. *Operations research* 52(1):35–53.
- Bertsimas D, Thiele A (2006) Robust and data-driven optimization: modern decision making under uncertainty. *Models, methods, and applications for innovative decision making*, 95–122 (INFORMS).
- Bertsimas D, Tsitsiklis JN (1997) *Introduction to linear optimization*, volume 6 (Athena scientific Belmont, MA).
- Chan T, Delage E, Lin B (2024) Conformal inverse optimization for adherence-aware prescriptive analytics. *Available at SSRN* .
- Chan TC, Mahmood R, Zhu IY (2025) Inverse optimization: Theory and applications. *Operations Research* 73(2):1046–1074.
- Chen S, Fioretto F, Qiu F, Zhu S (2025) Global-decision-focused neural odes for proactive grid resilience management. *arXiv preprint arXiv:2502.18321* .
- Cortes-Gomez S, Patiño C, Byun Y, Wu S, Horvitz E, Wilder B (2024) Decision-focused uncertainty quantification. *arXiv preprint arXiv:2410.01767* .
- Cresswell JC, Sui Y, Kumar B, Vouitsis N (2024) Conformal prediction sets improve human decision making. *Forty-first International Conference on Machine Learning*.
- DeCarolis JF (2011) Using modeling to generate alternatives (mga) to expand our thinking on energy futures. *Energy Economics* 33(2):145–152.
- Delage E, Ye Y (2010) Distributionally robust optimization under moment uncertainty with application to data-driven problems. *Operations research* 58(3):595–612.
- Delarue A, Lian Z, Martin S (2025) Algorithmic precision and human decision: A study of interactive optimization for school schedules. *Management Science* .

- Diamond S, Boyd S (2016) CVXPY: A Python-embedded modeling language for convex optimization. *Journal of Machine Learning Research* 17(83):1–5.
- Dietvorst BJ, Simmons JP, Massey C (2018) Overcoming algorithm aversion: People will use imperfect algorithms if they can (even slightly) modify them. *Management science* 64(3):1155–1170.
- Elmachtoub AN, Grigas P (2022) Smart “predict, then optimize”. *Management Science* 68(1):9–26.
- Fukuda K (1997) cdd/cdd+ reference manual. *Institute for Operations Research, ETH-Zentrum* 91–111.
- Fukuda K, Prodon A (1995) Double description method revisited. *Franco-Japanese and Franco-Chinese conference on combinatorics and computer science*, 91–111 (Springer).
- Gauthier E, Bach F, Jordan MI (2025a) Backward conformal prediction. *arXiv preprint arXiv:2505.13732* .
- Gauthier E, Bach F, Jordan MI (2025b) E-values expand the scope of conformal prediction. *arXiv preprint arXiv:2503.13050* .
- Grand-Clément J, Pauphilet J (2024) The best decisions are not the best advice: Making adherence-aware recommendations. *Management Science* .
- Grünwald P, de Heide R, Koolen W (2024) Safe testing. *Journal of the Royal Statistical Society Series B: Statistical Methodology* 86(5):1091–1128.
- Hullman J, Wu Y, Xie D, Guo Z, Gelman A (2025) Conformal prediction and human decision making. *arXiv preprint arXiv:2503.11709* .
- Ibrahim R, Kim SH, Tong J (2021) Eliciting human judgment for prediction algorithms. *Management Science* 67(4):2314–2325.
- Iyengar G, Kang W (2005) Inverse conic programming with applications. *Operations Research Letters* 33(3):319–330.
- Izbicki R, Shimizu G, Stern RB (2022) Cd-split and hpd-split: Efficient conformal regions in high dimensions. *Journal of Machine Learning Research* 23(87):1–32.
- Kim K, Mehrotra S (2015) A two-stage stochastic integer programming approach to integrated staffing and scheduling with application to nurse management. *Operations Research* 63(6):1431–1451.
- Kingma DP, Welling M (2013) Auto-encoding variational bayes. *arXiv preprint arXiv:1312.6114* .

- Kiyani S, Pappas G, Roth A, Hassani H (2025) Decision theoretic foundations for conformal prediction: Optimal uncertainty quantification for risk-averse agents. *arXiv preprint arXiv:2502.02561* .
- Kleywegt AJ, Shapiro A, Homem-de Mello T (2002) The sample average approximation method for stochastic discrete optimization. *SIAM Journal on optimization* 12(2):479–502.
- Kochenderfer MJ (2015) *Decision making under uncertainty: theory and application* (MIT press).
- Krein M, Milman D (1940) On extreme points of regular convex sets. *Studia Mathematica* 9:133–138.
- Lan H, Liao L, Elmachtoub AN, Kroer C, Lam H, Zhang H (2025) The bias-variance tradeoff in data-driven optimization: A local misspecification perspective. *arXiv preprint arXiv:2510.18215* .
- Li ML, Zhu S (2024) Balancing optimality and diversity: Human-centered decision making through generative curation. *arXiv preprint arXiv:2409.11535* .
- Lin B, Delage E, Chan T (2024) Conformal inverse optimization. *Advances in Neural Information Processing Systems* 37:63534–63564.
- Lombardi F, van Greevenbroek K, Grochowicz A, Lau M, Neumann F, Patankar N, Vågerö O (2025) Near-optimal energy planning strategies with modeling to generate alternatives to flexibly explore practically desirable options. *Joule* .
- Mandi J, Kotary J, Berden S, Mulamba M, Bucarey V, Guns T, Fioretto F (2024) Decision-focused learning: Foundations, state of the art, benchmark and future opportunities. *Journal of Artificial Intelligence Research* 80:1623–1701.
- Motzkin TS, Raiffa H, Thompson GL, Thrall RM (1953) The double description method. *Contributions to the Theory of Games* 2(28):51–73.
- Orfanoudaki A, Saghafian S, Song K, Chakkera HA, Cook C (2022) Algorithm, human, or the centaur: How to enhance clinical care? .
- Palminier B (2014) Flexibility in generation planning: Identifying key operating constraints. *2014 power systems computation conference*, 1–7 (IEEE).
- Papadopoulos H, Proedrou K, Vovk V, Gammerman A (2002) Inductive confidence machines for regression. *Machine learning: ECML 2002: 13th European conference on machine learning Helsinki, Finland, August 19–23, 2002 proceedings 13*, 345–356 (Springer).

- Parenti N, Reggiani MLB, Iannone P, Percudani D, Dowding D (2014) A systematic review on the validity and reliability of an emergency department triage scale, the manchester triage system. *International Journal of Nursing Studies* 51(7):1062–1069, ISSN 0020-7489, URL <http://dx.doi.org/https://doi.org/10.1016/j.ijnurstu.2014.01.013>.
- Pedregosa F, Varoquaux G, Gramfort A, Michel V, Thirion B, Grisel O, Blondel M, Prettenhofer P, Weiss R, Dubourg V, et al. (2011) Scikit-learn: Machine learning in python. *the Journal of machine Learning research* 12:2825–2830.
- Prinster D, Saria S, Liu A (2023) Jaws-x: addressing efficiency bottlenecks of conformal prediction under standard and feedback covariate shift. *International Conference on Machine Learning*, 28167–28190 (PMLR).
- Rahimian H, Mehrotra S (2022) Frameworks and results in distributionally robust optimization. *Open Journal of Mathematical Optimization* 3:1–85.
- Schaefer AJ (2009) Inverse integer programming. *Optimization Letters* 3:483–489.
- Shafer G, Vovk V (2008) A tutorial on conformal prediction. *Journal of Machine Learning Research* 9(3).
- Shapiro A, Dentcheva D, Ruszczyński A (2021) *Lectures on stochastic programming: modeling and theory* (SIAM).
- Singh S, Sarna N, Li Y, Lin Y, Orfanoudaki A, Berger M (2024) Distribution-free risk assessment of regression-based machine learning algorithms. *The 13th Symposium on Conformal and Probabilistic Prediction with Applications*, 44–64 (PMLR).
- Tao PD, An LH (1997) Convex analysis approach to dc programming: theory, algorithms and applications. *Acta mathematica vietnamica* 22(1):289–355.
- Tavaslıoğlu O, Lee T, Valeva S, Schaefer AJ (2018) On the structure of the inverse-feasible region of a linear program. *Operations Research Letters* 46(1):147–152.
- Tian X, Yan R, Liu Y, Wang S (2023) A smart predict-then-optimize method for targeted and cost-effective maritime transportation. *Transportation Research Part B: Methodological* 172:32–52.
- Topkis DM (1998) *Supermodularity and complementarity* (Princeton university press).
- Vovk V (2025) Conformal e-prediction. *Pattern Recognition* 111674.
- Vovk V, Gammerman A, Shafer G (2005) *Algorithmic learning in a random world*, volume 29 (Springer).

- Wang Z, Gao R, Yin M, Zhou M, Blei D (2023) Probabilistic conformal prediction using conditional random samples. *International Conference on Artificial Intelligence and Statistics*, 8814–8836 (PMLR).
- Wright SJ (2015) Coordinate descent algorithms. *Mathematical programming* 151(1):3–34.
- Zhang Z, Shi P, Ward A (2025) Admission decisions under imperfect classification: An application in criminal justice. *Available at SSRN 5214197* .
- Zheng M, Zhu S (2024) Generative conformal prediction with vectorized non-conformity scores. *arXiv preprint arXiv:2410.13735* .
- Zhou W, Zhu S, Qiu F, Wu X (2024) Hierarchical spatio-temporal uncertainty quantification for distributed energy adoption. *arXiv preprint arXiv:2411.12193* .
- Zhu S, Wang H, Xie Y (2022) Data-driven optimization for atlanta police-zone design. *INFORMS Journal on Applied Analytics* 52(5):412–432.

Appendix A: Proofs

A.1. Proof of Theorem 1

In this section, we denote k -th prediction set constructed by $\hat{y}^{(k)}$ as $C^k(\cdot; \cdot)$ for notation clarity.

LEMMA 3 (E-value post-hoc validity). *Denote the k -th prediction set constructed by $\hat{y}^{(k)}$ as C^k . Then under Assumption 1,*

$$\mathbb{P}\{Y \in C^{(k)}(X; \hat{\alpha})\} \geq 1 - \mathbb{E}[\hat{\alpha}], \quad \forall k = 1, \dots, K.$$

where $\hat{\alpha}$ is some arbitrary function of $\{(X_i, Y_i)\}_{i=1}^{n+1}$.

Proof of Lemma 3 When $\hat{\alpha} < 1/(n+1)$ or $\hat{\alpha} = 1$, by the definition of all three variants of $R(\alpha)$, the statement holds trivially. So we only need to consider the case when $1 > \hat{\alpha} \geq 1/(n+1)$. For any $k = 1, \dots, K$, we begin by expanding the left-hand side:

$$\begin{aligned} \mathbb{P}\{Y \notin C^{(k)}(X; \hat{\alpha})\} &= \mathbb{P}\left\{\|\hat{y}^{(k)} - Y\|_2 > \frac{\sum_{i=1}^n \|\hat{y}_i - Y_i\|_2}{\hat{\alpha}(n+1) - 1}\right\} \\ &= \mathbb{P}\left\{\hat{\alpha}(n+1)\|Y - \hat{y}^{(k)}\|_2 > \sum_{i=1}^n \|\hat{y}_i - Y_i\|_2 + \|\hat{y}^{(k)} - Y\|_2\right\} \\ &= \mathbb{P}\left\{\hat{\alpha} > \frac{\sum_{i=1}^n \|\hat{y}_i - Y_i\|_2 + \|\hat{y}^{(k)} - Y\|_2}{(n+1)\|\hat{y}^{(k)} - Y\|_2}\right\} \\ &= \mathbb{P}\left\{\frac{(n+1)\|\hat{y}^{(k)} - Y\|_2}{\sum_{i=1}^n \|\hat{y}_i - Y_i\|_2 + \|\hat{y}^{(k)} - Y\|_2} > \frac{1}{\hat{\alpha}}\right\}. \end{aligned}$$

Denote the following random variables,

$$\begin{aligned} F_i &= \frac{(n+1)\|\hat{y}_i - Y_i\|_2}{\sum_{i=1}^n \|\hat{y}_i - Y_i\|_2 + \|\hat{y}^{(k)} - Y\|_2}, \quad \forall i = 1, \dots, n, \\ F_{n+1} &= \frac{(n+1)\|\hat{y}^{(k)} - Y\|_2}{\sum_{i=1}^n \|\hat{y}_i - Y_i\|_2 + \|\hat{y}^{(k)} - Y\|_2}. \end{aligned}$$

It can be seen that the following two conditions hold:

$$\begin{aligned} (a): \quad & \mathbb{E}[F_1 + \dots + F_n + F_{n+1}] = n + 1, \\ (b): \quad & \mathbb{E}[F_1] = \dots = \mathbb{E}[F_n] = \mathbb{E}[F_{n+1}], \end{aligned}$$

where (b) holds by exchangeability (Assumption 1). Therefore, there is

$$\mathbb{E}[F_{n+1}] = 1. \tag{20}$$

Using this result, it can be derived that

$$\sup_{\tilde{\alpha}} \mathbb{E}\left[\frac{\mathbb{P}(F_{n+1} > 1/\tilde{\alpha})}{\tilde{\alpha}}\right] \leq \sup_{\tilde{\alpha}} \mathbb{E}\left[\frac{\tilde{\alpha} \cdot \mathbb{E}[F_{n+1}]}{\tilde{\alpha}}\right] = \mathbb{E}[F_{n+1}] = 1,$$

where the inequality follows from Markov's inequality. Therefore, for any $\hat{\alpha}$ which may depend on the data $\{X_i, Y_i\}_{i=1}^{n+1}$, there is:

$$\mathbb{E} \left[\frac{\mathbb{P}(F_{n+1} > 1/\hat{\alpha} \mid \hat{\alpha})}{\hat{\alpha}} \right] \leq \sup_{\tilde{\alpha}} \mathbb{E} \left[\frac{\mathbb{P}(F_{n+1} > 1/\tilde{\alpha})}{\tilde{\alpha}} \right] \leq 1$$

Using a first-order Taylor expansion on the left-hand side of the inequality above, there is

$$\mathbb{E} \left[\frac{\mathbb{P}(F_{n+1} > 1/\hat{\alpha} \mid \hat{\alpha})}{\hat{\alpha}} \right] \approx \frac{\mathbb{E} [\mathbb{P}(F_{n+1} > 1/\hat{\alpha} \mid \hat{\alpha})]}{\mathbb{E}[\hat{\alpha}]} \quad (21)$$

We assume that this approximation is exact, so the \approx sign can be replaced with a $=$ sign. Consequently, by combining the two equations above, we get

$$\mathbb{E} [\mathbb{P}(F_{n+1} > 1/\hat{\alpha} \mid \hat{\alpha})] \leq \mathbb{E}[\hat{\alpha}] \iff \mathbb{P} \{y \in C^{(k)}(x; \hat{\alpha})\} \geq 1 - \mathbb{E}[\hat{\alpha}],$$

where $\hat{\alpha}$ can probabilistically depend on $\{(X_i, Y_i)\}_{i=1}^{n+1}$ in arbitrary ways. \square

Proof of Theorem 1 We begin by noticing the following decomposition

$$\mathbb{P} \{z \in \pi(Y)\} = \mathbb{P} \{Y \in \pi^{-1}(z)\} \geq \frac{1}{K} \sum_{k=1}^K \mathbb{P} \{Y \in C^{(k)}(X; \tilde{\alpha}^{(k)}(z))\}. \quad (22)$$

The first equality follows from our problem reformulation (Lemma 1). The second inequality holds due to the definition of $\tilde{\alpha}^{(k)}(z)$, which guarantees that the k -th generated CP region is always contained in $\pi^{-1}(z)$. Since by Lemma 3, we have proved that:

$$\mathbb{P} \{Y \in C^{(k)}(X; \tilde{\alpha}^{(k)}(z))\} \geq 1 - \mathbb{E} [\tilde{\alpha}^{(k)}(z)].$$

Therefore, combining this with (22) we obtain:

$$\mathbb{P} \{z \in \pi(Y)\} \geq 1 - \mathbb{E} \left[\frac{1}{K} \sum_{k=1}^K \tilde{\alpha}^{(k)}(z) \right] = 1 - \mathbb{E} [\hat{\alpha}(z)].$$

We conclude the entire proof for Theorem 1.

REMARK 2 (DISCUSSION ON THE TAYLOR APPROXIMATION ERROR). We comment on the approximation error of the first-order Taylor approximation in (21). This approximation trick has been adopted in prior works (Gauthier et al. 2025b), which has been argued that its error is small when the estimator $\hat{\alpha}$ is well concentrated around its mean. Empirically, this condition is usually satisfied in our setting. For example, when CREDO is deployed in a human-algorithm collaboration setting, the candidate decisions provided from the decision maker would be expected to be near optimal and should already enjoy a relatively small ground truth risk. This makes $\hat{\alpha}$ have a relatively small variance and well concentrated around its mean.

Even when this condition does not hold, we can resort to an alternative way to account for the approximation error during risk assessment. This can be done by theoretically deriving the approximation error and then manually offsetting the error in our risk estimator to achieve an exact conservativeness guarantee. Specifically, let $h(\hat{\alpha}) := \mathbb{E}[\mathbb{P}(F_{n+1} > 1/\hat{\alpha} \mid \hat{\alpha})]$, there is:

$$\left| \mathbb{E} \left[\frac{h(\hat{\alpha})}{\hat{\alpha}} \right] - \frac{\mathbb{E}[h(\hat{\alpha})]}{\mathbb{E}[\hat{\alpha}]} \right| \leq \mathbb{E}[h(\hat{\alpha})] \left(\mathbb{E} \left[\frac{1}{\hat{\alpha}} \right] - \frac{1}{\mathbb{E}[\hat{\alpha}]} \right) + \sqrt{\text{Var}(h(\hat{\alpha})) \cdot \text{Var} \left(\frac{1}{\hat{\alpha}} \right)}.$$

The first term is the Jensen gap, and the second term is by the Cauchy-Schwarz inequality. Assuming $\hat{\alpha} \in [\delta, 1]$ almost surely, then

$$\mathbb{E} \left[\frac{1}{\hat{\alpha}} \right] - \frac{1}{\mathbb{E}[\hat{\alpha}]} \leq \frac{1}{\delta^3} \text{Var}(\hat{\alpha}), \quad \text{and} \quad \text{Var} \left(\frac{1}{\hat{\alpha}} \right) \leq \frac{1}{\delta^3} \text{Var}(\hat{\alpha}).$$

Then, plugging them into the previous equation, we get

$$\left| \mathbb{E} \left[\frac{h(\hat{\alpha})}{\hat{\alpha}} \right] - \frac{\mathbb{E}[h(\hat{\alpha})]}{\mathbb{E}[\hat{\alpha}]} \right| \leq \frac{1}{\delta^3} \text{Var}(\hat{\alpha}) + \frac{1}{2\delta^2} \sqrt{\text{Var}(\hat{\alpha})}.$$

Since for random variables bounded within $[\delta, 1]$, there is the following trivial upper bound:

$$\text{Var}(\hat{\alpha}) \leq \frac{1}{K^2} \sum_{k,k'} \text{Cov}(I_k, I'_k) \leq \frac{1}{4},$$

therefore, we can conclude that:

$$\left| \mathbb{E} \left[\frac{\mathbb{P}(F_{n+1} > 1/\hat{\alpha} \mid \hat{\alpha})}{\hat{\alpha}} \right] - \frac{\mathbb{E}[\mathbb{P}(F_{n+1} > 1/\hat{\alpha} \mid \hat{\alpha})]}{\mathbb{E}[\hat{\alpha}]} \right| \leq \frac{1}{4\delta^3} + \frac{1}{4\delta^2}.$$

Plugging this result back into the proof of Theorem 1, we get

$$\mathbb{P}\{z \in \pi(Y)\} \geq 1 - \mathbb{E}[\hat{\alpha}(z)] - 1/4(\delta^{-3} + \delta^{-2}).$$

Therefore, one can take the final estimator as

$$\min\{\hat{\alpha}(z) + 1/4(\delta^{-3} + \delta^{-2}), 1\} \tag{23}$$

so that exact conservativeness is achieved. A trivial value that the user can take for δ is $1/(n+1)$, which is guaranteed by the design of the CREDO algorithm. One can also manually tune the value of δ by modifying the calibrated radius as

$$R'(\alpha) = \begin{cases} +\infty, & \text{if } \alpha \in [0, \delta), \\ R(\alpha) & \text{if } \alpha \in [\delta, 1), \\ 0 & \text{if } \alpha = 1, \end{cases}$$

to achieve a tighter bound (*i.e.*, smaller offset). One can prove that as long as δ is chosen such that $\delta > 1/(n+1)$, all theorems presented in the main text remain valid, and the bound (*i.e.*, offset) becomes tighter as δ increases. Then,

one can adopt $R'(\alpha)$ as the conformalized radius and take (23) as the final estimator. This procedure is equivalent to truncating the lower part of $\hat{\alpha}(z)$ at δ , *i.e.*, setting $\max\{\hat{\alpha}(z), \delta\}$ as the risk estimator, and then taking (23) as the final estimator, which is simpler to execute in implementation.

A.2. Proof of Corollary 1

Proof The proof mainly follows the proof of Theorem 1 in Barber et al. (2023), with the exception that all steps are conditioned on the σ -field generated by $\tilde{\alpha}^{(k)}(z)$ ⁴. Following the proof of Theorem 1 in Barber et al. (2023), we can derive that:

$$\mathbb{P}\left[Y \in C^{(k)}(X; \tilde{\alpha}^{(k)}(z)) \mid \tilde{\alpha}^{(k)}(z)\right] \geq 1 - \alpha - \frac{\sum_{i=1}^n d_{\text{TV}}^{(i)}(\hat{\alpha}(z))}{n+1}.$$

Plugging this equation back in (22), we get

$$\mathbb{P}\{\pi(Y) = z\} \geq 1 - \frac{1}{K} \sum_{k=1}^K \mathbb{E} \left[\tilde{\alpha}^{(k)}(z) + \frac{\sum_{i=1}^n \mathbb{E} \left[d_{\text{TV}}^{(i)}(\hat{\alpha}(z)) \right]}{n+1} \right] = 1 - \mathbb{E}[\tilde{\alpha}(z)] - \frac{\sum_{i=1}^n d_{\text{TV}}^{(i)}(\hat{\alpha}(z))}{n+1}.$$

The expectations are taken with respect to all sources of randomness of $\tilde{\alpha}^{(k)}(z)$. □

A.3. Proof of Proposition 1

Proof By Remark 1,

$$\hat{\alpha}(z) = 1 - \frac{1}{K} \sum_{k=1}^K \mathbb{1}\{\hat{y}^{(k)} \in \pi^{-1}(z)\}.$$

Therefore, for any $x \in \mathcal{X}$, conditioning on $X = x$, there is

$$\begin{aligned} |\hat{\alpha}(z) - \mathbb{P}\{z \in \pi(Y) \mid X = x\}| &= 1 - \frac{1}{K} \sum_{k=1}^K \left(\mathbb{1}\{\hat{y}^{(k)} \in \pi^{-1}(z)\} - \mathbb{P}\{z \in \pi(Y) \mid X = x\} \right) - 1 \\ &= \frac{1}{K} \sum_{k=1}^K \left(\mathbb{1}\{\hat{y}^{(k)} \in \pi^{-1}(z)\} - \mathbb{P}\{z \in \pi(Y) \mid Y \sim \mathcal{P}_{\mathcal{Y} \mid X=x}\} \right) \\ &= \frac{1}{K} \sum_{k=1}^K \underbrace{\left(\mathbb{1}\{\hat{y}^{(k)} \in \pi^{-1}(z)\} - \mathbb{P}\{z \in \pi(Y) \mid Y \sim \hat{\mathcal{P}}_{\mathcal{Y} \mid X=x}\} \right)}_{T_k^{(1)}} + \\ &\quad \frac{1}{K} \sum_{k=1}^K \underbrace{\left(\mathbb{P}\{z \in \pi(Y) \mid Y \sim \hat{\mathcal{P}}_{\mathcal{Y} \mid X=x}\} - \mathbb{P}\{z \in \pi(Y) \mid Y \sim \mathcal{P}_{\mathcal{Y} \mid X=x}\} \right)}_{T_k^{(2)}} \\ &= \frac{1}{K} \sum_{k=1}^K T_k^{(1)} + \frac{1}{K} \sum_{k=1}^K T_k^{(2)}. \end{aligned}$$

⁴ We note that the σ -field generated by $\tilde{\alpha}^{(k)}(z)$ is the same across all k , as they are just different simulation trials based on the same input and generative model, therefore they are equal to the σ -field of $\hat{\alpha}(z)$.

For the first term, since $T_k^{(1)}$ are i.i.d. random variables⁵, and $\mathbb{E}[T_k^{(1)} | X = x] = 0$, assuming that its variance is finite, by the central limit theorem, there is $\frac{1}{K} \sum_{k=1}^K T_k^{(1)} = O_p(K^{-1/2})$. For the second term, note that by the assumption

$$T_k^{(2)} = \mathbb{P}\{Y \in \pi^{-1}(z) | Y \sim \hat{\mathcal{P}}_{Y|X=x}\} - \mathbb{P}\{Y \in \pi^{-1}(z) | Y \sim \mathcal{P}_{Y|X=x}\} \leq d_{TV}(\hat{\mathcal{P}}_{Y|X=x}, \mathcal{P}_{Y|X=x}) \leq \delta,$$

where the first inequality follows from the definition of total variation distance. Therefore, we conclude that

$$|\hat{\alpha}(z) - \mathbb{P}\{z \in \pi(Y) | X = x\}| = O_p(K^{-1/2}) + \delta.$$

□

A.4. Proof of Proposition 2

Proof For notation simplicity, denote the sets in the numerator and the denominator of TPR defined in (13) as:

$$A = \{z \in \mathcal{Z} | \mathbb{P}\{z \notin \pi(Y)\} < 1 \text{ and } \hat{\alpha}(z) < 1\},$$

$$B = \{z \in \mathcal{Z} | \mathbb{P}\{z \notin \pi(Y)\} < 1\}.$$

Note that $A \subseteq B$. Without loss of generality, we assume that B (therefore A) is a finite set, *i.e.*, there is only a finite set of decisions that have ground-truth risk smaller than one⁶. We also define

$$w^{(k)} := 1 - R^{-1} \left(\min_{y \in \partial \pi^{-1}(z)} \|\hat{y}^{(k)} - y\|_2 \right).$$

Since B is a constant irrelevant to K , we begin by expanding the following expression:

$$\begin{aligned} \mathbb{E}[\#A] &= \mathbb{E} \left[\sum_{z \in B} \mathbb{1}\{\hat{\alpha}(z) < 1\} \right] \\ &= \mathbb{E} \left[\sum_{z \in B} \left(1 - \prod_{k=1}^K \left(\mathbb{1}\{\hat{y}_{n+1}^{(k)} \notin \pi^{-1}(z)\} \cdot \mathbb{1}\{w^{(k)} > 0\} \right) \right) \right] \\ &= \mathbb{E}[\#B] - \mathbb{E} \left[\sum_{z \in B} \prod_{k=1}^K A_k \right]. \end{aligned}$$

Here, the second equality results from the observation that when: (i) at least one of the model predictions falls within $\pi^{-1}(z)$, and (ii) its calibrated weight is not zero, then the estimated risk after averaging would be less than one. In the last equality, we denote

$$A_k = \mathbb{1}\{\hat{y}^{(k)} \notin \pi^{-1}(z)\} \cdot \mathbb{1}\{w^{(k)} > 0\}.$$

⁵ Since $\hat{y}^{(k)}$ are independently generated from the same generative model given x .

⁶ This proof naturally extends to the infinite case by replacing the counting measure “#” with continuous measures, such as Lebesgue measure defined within the decision space \mathcal{Z} .

Note that $A_k \in \{0, 1\}$ and has a nonzero probability taking one⁷. Since at the right hand side, the term $\prod_{k=1}^K A_k$ monotonically decreases with K almost surely, then $\mathbb{E}[\#A]$ monotonically increase with K . Since $\text{TPR} = \mathbb{E}[\#A] / \mathbb{E}[\#B]$, we know that TPR monotonically increases with K . This concludes the proof.

A.5. Proof of Proposition 3

Proof We begin by noticing that the set containment condition $C(x; \alpha) \subseteq \pi^{-1}(z)$ is equivalent to requiring that the calibrated conformal ball does *not* intersect the complement of the inverse feasible region:

$$C(x; \alpha) \subseteq \pi^{-1}(z) \iff C(x; \alpha) \cap (\pi^{-1}(z))^c = \emptyset.$$

Since $C(x; \alpha)$ is an ℓ_2 ball centered at \hat{y} , the right hand side is further equivalent to

$$\underbrace{\text{for all } y \in (\pi^{-1}(z))^c, \|y - \hat{y}\|_2 \geq R(\alpha)}_{(i)} \quad \text{if } \underbrace{\hat{y} \in \pi^{-1}(z)}_{(ii)}. \quad (24)$$

Here, condition (i) requires that every scenario y violating the optimality of decision z must lie at least with distance $R(\alpha)$ away from \hat{y} ; condition (ii) states that the former condition is enforced only when \hat{y} lies within of $\pi^{-1}(z)$. Otherwise, then no radius can guarantee containment, and the α is trivially mapped to one by design. Therefore under (ii), (11) can be reformulated as

$$\min_{\alpha} \max_y \alpha \quad \text{s.t.} \quad \|y - \hat{y}\|_2 \geq R(\alpha) \quad \text{and} \quad y \in (\pi^{-1}(z))^c. \quad (25)$$

Since by the monotonicity of R , there is

$$\|y - \hat{y}\|_2 \geq R(\alpha) \iff \alpha \geq R^{-1}(\|y - \hat{y}\|_2),$$

so the first constraint in (25) can be replaced as

$$\min_{\alpha} \max_y \alpha \quad \text{s.t.} \quad \alpha \geq R^{-1}(\|y - \hat{y}\|_2) \quad \text{and} \quad y \in (\pi^{-1}(z))^c,$$

which makes α a slack variable that can be dropped by moving the constraint expression to the objective:

$$\max_y R^{-1}(\|y - \hat{y}\|_2) \quad \text{s.t.} \quad y \in (\pi^{-1}(z))^c.$$

Finally, by definition of π^{-1} , the constraint can be expanded as

$$y \in (\pi^{-1}(z))^c \iff f(z; y) > \min_{z' \in \mathcal{Z}} f(z'; y) + \epsilon.$$

Plugging this constraint into the optimization above yields the desired statement. \square

⁷ Under some regularity condition on the distribution of Y , e.g., is supported on the whole space \mathcal{Y} . Without this condition, the statement also holds by changing “monotonically increasing” to “non-decreasing”.

A.6. Proof of Proposition 4

Proof We begin the derivation by expanding the indicator term:

$$\begin{aligned}
 \mathbb{1} \{y \in \pi^{-1}(z)\} &= \mathbb{1} \left\{ f(y, z) \leq \min_{z' \in \mathcal{Z}} f(y, z'; \theta) + \epsilon \right\} \\
 &= \prod_{z' \in \mathcal{Z}} \mathbb{1} \{f(y, z) \leq f(y, z') + \epsilon\} \\
 &= \prod_{z' \in \mathcal{Z}} \mathbb{1} \{\langle y, z - z' \rangle \leq \epsilon\} \\
 &= \mathbb{1} \left\{ \max_{z' \in \mathcal{Z}} \langle y, z - z' \rangle \leq \epsilon \right\}
 \end{aligned}$$

Since \mathcal{Z} is a compact set, by the Krein–Milman theorem (Krein and Milman 1940), there is

$$\max_{z' \in \mathcal{Z}} \langle y, z - z' \rangle = \max_{v \in \mathcal{V}} \langle y, z - v \rangle.$$

Plugging this into the tight hand side of the derivation above, we get

$$\mathbb{1} \left\{ \max_{z' \in \mathcal{Z}} \langle y, z - z' \rangle \leq \epsilon \right\} = \prod_{v \in \mathcal{V}} \mathbb{1} \{\langle y, z - v \rangle \leq \epsilon\}.$$

Therefore, we conclude that

$$\mathbb{1} \{\hat{y}^{(k)} \in \pi^{-1}(z)\} = \prod_{v \in \mathcal{V}} \mathbb{1} \{\langle \hat{y}^{(k)}, z - v \rangle \leq 0\}.$$

Combining the above statement with Proposition 3, (19) can be expanded as

$$\min_y \|y - \hat{y}\|_2 \quad \text{s.t.} \quad \max_{v \in \mathcal{V}} \langle \hat{y}, z - v \rangle \leq 0$$

This is the optimization of finding the closest distance from a point \hat{y} to a cone formed by the intersections of halfspaces.

By using the well-known point to halfspace distance formula and rearranging the notations, we obtain the desired statement. \square

Appendix B: Experiment Details

This section is organized as follows: Section B.1 shows the computation resources used in our experiments. Section B.2 and Section B.3 presents the detailed configurations for the two synthetic settings and the real-world case study, respectively. Section B.4 describes the detailed configurations of CREDO, the baselines, and the procedures for the two experiments (Conservativeness versus Accuracy Tradeoff and Decision Quality Evaluation).

Table 4 Computation resources specifications

Operating System	CPU	RAM	GPU
Windows 11	13th-generation Intel Core i7, 16 cores	16GB	Not used

B.1. Computation Resources

The computational resources used in our experiments are detailed in Table 4. Our code is implemented in Python, with key dependencies including Scikit-learn (Pedregosa et al. 2011) for solving linear programs and working with Gaussian mixture models (fitting and sampling), and CDD (Fukuda 1997) for computing the vertices of polytopes. We also use `cvxpy` (Diamond and Boyd 2016) and `cvxpylayers` (Agrawal et al. 2019) libraries to solve convex optimization problems and implement differentiable optimization layers. We use the default parameter settings in their libraries across all experiments. A complete list of dependencies and their version numbers is available in our codebase.

B.2. Synthetic Setting

We denote σ as the component variance scale ($\sigma = 1$ by default), and we denote \mathbf{I}_2 as the two-dimensional identity matrix.

Setting I A linear programming problem featuring a triangular feasible region with three vertex decisions, defined as:

$$\max_{z \in \mathbb{R}^2} \{Y_1 z_1 + Y_2 z_2 \mid z_1 + z_2 \leq 1, z_i \geq 0, z_2 \geq 0\}, \quad \begin{pmatrix} Y_1 \\ Y_2 \end{pmatrix} \sim \mathcal{N}\left(\begin{pmatrix} -1 \\ -1 \end{pmatrix}, \sigma \cdot \mathbf{I}_2\right).$$

This optimization problem can be interpreted as a profit maximization task, where a manufacturer chooses the optimal production quantities z_1 and z_2 under a budget constraint. The Gaussian random revenues Y_1 and Y_2 have negative expected values but may exhibit some variance, capturing a risky market scenario that could still yield profit under favorable conditions.

The feasible region in this problem can be more compactly denoted by its constraint matrix \mathbf{A} and constraint vector \mathbf{b} as

$$\mathbf{A} = \begin{pmatrix} 1 & 1 \\ -1 & 0 \\ 0 & -1 \end{pmatrix} \quad \mathbf{b} = \begin{pmatrix} 1 \\ 0 \\ 0 \end{pmatrix}.$$

Setting II A linear programming problem that employs a more complex octagonal feasible region with five vertices and multimodal objective uncertainty, allowing us to assess performance in scenarios with multiple potentially optimal

decisions. Specifically, the optimization problem is set up as the canonical form $\max_{z \in \mathbb{R}^2} \{Y^\top z \mid \mathbf{A}z \leq \mathbf{b}\}$, where the constraint matrices \mathbf{A} and constraint vector \mathbf{b} are defined as

$$\mathbf{A} = \begin{pmatrix} -0.5 & -1 \\ 0 & -1 \\ -0.5 & 1 \\ 0.5 & 1 \\ 2 & -1 \\ 1 & 0 \\ 0 & 1 \\ -1 & 0 \end{pmatrix} \quad \mathbf{b} = \begin{pmatrix} -1 \\ 0 \\ 1 \\ 5 \\ 10 \\ 5.5 \\ 2.5 \\ -1 \end{pmatrix}.$$

The random vector $Y \in \mathbb{R}^2$ is drawn from a three-component Gaussian mixture distribution

$$p(x) = \sum_{k=1}^3 w_k \mathcal{N}\left(x \mid \mu_k, \sigma \cdot \sigma_k^2 \mathbf{I}_2\right),$$

where the mixture weights are $\mathbf{w} = (0.3, 0.4, 0.3)$, the component means are

$$\mu_1 = \begin{pmatrix} 0.00.8 \end{pmatrix}, \quad \mu_2 = \begin{pmatrix} -0.5 & .25 \end{pmatrix}, \quad \mu_3 = \begin{pmatrix} 0.80.1 \end{pmatrix},$$

and the component variances are

$$\sigma_1^2 = (0.01)^2, \quad \sigma_2^2 = (0.03)^2, \quad \sigma_3^2 = (0.02)^2.$$

B.3. Real-World Setting

As described in the main paper, we consider a real-world power grid investment decision-making problem (Zhou et al. 2024). We begin by introducing the application background, followed by a formalization of the problem as a knapsack optimization. Finally, we present a linear programming relaxation of this problem, which can be directly used in CREDO.

Background A utility company based in Indianapolis, Indiana, has compiled detailed records of over 1,700 solar panel installations between 2010 and 2024, including the installation dates and affiliated grid components. With the renewable energy sector now at full scale, the management team anticipates a steady and significant monthly increase in solar adoption in the downtown area. In preparation for the incoming demand, they are planning targeted upgrades to grid-level inverters at four selected substations (we refer to them as Substation A to D) under a limited budget. The

utility company would like to consult on CREDO’s suggestion for a list of candidate upgrade plans that would most likely be optimal.

The data is available in our codebase in a spatio-temporally aggregated format (monthly, by substation), with substation names anonymized. However, the granular solar panel installation data used in this study cannot be shared publicly, as it is proprietary to the utility company.

Mathematical Formulation This problem can be mathematically formulated as a penalized knapsack problem, whose goal is to minimize the total penalty from capacity violations while ensuring that the total upgrade cost does not exceed the budget. Formally, define d as the total number of substations, and define parameters as in Table 5, the optimization problem can be written as

$$\min_{\mathbf{a} \in \{0,1\}^d} \sum_{i=1}^d \mathbb{1}(Y_i \geq \tau_i)(1 - a_i)l_i \quad \text{s.t.} \quad \sum_{i=1}^d a_i c_i \leq b. \quad (26)$$

Table 5 Parameter definitions for the real-world optimization problem

Parameter	Definition
a_i	Binary decision variable; $a_i = 1$ indicates a substation upgrade, and $a_i = 0$ indicates no upgrade.
Y_i	Random variable representing the monthly increase in solar panel installations.
c_i	Cost associated with upgrading substation i .
τ_i	Capacity threshold—the maximum number of allowable solar connections at substation i .
l_i	Penalty incurred if the threshold τ_i is exceeded without an upgrade.
b	Total budget.

In our experiment, we configure these parameters as follows: we assume the cost c_i and loss l_i for all substations equals one unit. The capacity threshold τ_i is set to be the historical average solar panel monthly increment. The budget b

is set to half the cost of upgrading all substations, allowing at most two out of four substations can be upgraded. Note that these parameters require additional information from the company, which is not available at the time of writing this paper.

Relaxed Formulation The knapsack problem defined in (26) can be relaxed into the following linear programming problem:

$$\min_{z \in [0,1]^d} \sum_{i=1}^d \frac{l_i}{1 + e^{-\beta(Y_i - \tau_i)}} (1 - a_i) \quad \text{s.t.} \quad - \sum_{i=1}^d c_i z_i \leq b - \sum_{i=1}^d c_i, \quad (27)$$

where β is an arbitrary smoothing parameter that we set $\beta = 0.5$. Note that in the equation above, two relaxations have been applied:

- The binary random variable $\mathbb{1}\{Y_i \geq \tau_i\}$ has been relaxed to a continuous random variable over $[0, 1]$ using the sigmoid function, where the smoothing parameter β controls the sharpness of the approximation.
- The decision space of a_i has been relaxed from the discrete set $\{0, 1\}^d$ to the continuous unit hypercube $[0, 1]^d$.

This relaxation does not introduce approximation bias, as the optimal solutions to the original and relaxed problems are almost surely the same – both attained at one of the hypercube’s vertices.

Denote the vectors

$$Y = \begin{pmatrix} \frac{l_1}{1 + e^{-\beta(Y_1 - \tau_1)}} \\ \dots \\ \frac{l_d}{1 + e^{-\beta(Y_d - \tau_d)}} \end{pmatrix}, \quad \mathbf{c} = \begin{pmatrix} c_1 \\ \dots \\ c_d \end{pmatrix}, \quad \mathbf{z} = \begin{pmatrix} 1 - a_1 \\ \dots \\ 1 - a_d \end{pmatrix}, \quad (28)$$

we can compactly write the optimization problem above as

$$\min_{z \in \mathbb{R}^d} Y^\top z \quad \text{s.t.} \quad -\mathbf{c}^\top z \leq b - \mathbf{1}_d^\top \mathbf{c}, \quad \mathbf{0} \leq z \leq \mathbf{1}. \quad (29)$$

This can be written as the canonical form of linear programming $\min_{z \in \mathbb{R}^d} \{Y^\top z \mid \mathbf{A}z \leq \mathbf{b}\}$ by defining

$$\mathbf{A} = \begin{pmatrix} -\mathbf{c}^\top \\ \mathbf{I}_d \\ -\mathbf{I}_d \end{pmatrix}, \quad \mathbf{b} = \begin{pmatrix} b - \mathbf{1}_d^\top \mathbf{c} \\ \mathbf{1}_d \\ \mathbf{0}_d \end{pmatrix},$$

where \mathbf{I}_d denotes the d -dimensional identity matrix, and $\mathbf{1}_d$ and $\mathbf{0}_d$ denote the d -dimensional all-ones and all-zeros vectors, respectively. These parameters can be directly input to the CREDO framework using the data Y obtained via sigmoid transformation defined in (28) to obtain decision risk estimates.

B.4. Benchmarking Baselines Description

In this part, we describe the baselines, metrics, as well as the detailed evaluation procedure for each experiment that we conducted in the main paper. For both experiments, the following (Table 6) default values of hyperparameters are used for CREDO.

Table 6 Hyperparameters in the Conservativeness vs. Accuracy Tradeoff experiment.

Hyperparameter	Description	Default value
K	Simulation size	1×10^2
σ	(Component) variance scale	1
n	Calibration dataset size	1×10^1
m	Training dataset size	1×10^1

Table 7 summarizes the evaluation metrics used in our experiment. We use T to denote the total number of repeated independent trials, where we set $T = 20$ across all of our experiments. For each metric, the error is reported as the *standard error of the mean (SEM)*, calculated as the standard deviation of the metric values across trials divided by \sqrt{T} . Note that while most metrics require summing over all feasible decisions, we can simplify to summing all the decisions defined on the vertices of the feasible region, as we have justified in the main text.

Table 8 presents the four selected baselines used in the Decision Quality Evaluation experiment. The baselines have been selected to satisfy the following criteria: (i) the ability to produce a decision that maximizes a (linear) objective function; and (ii) the capacity to handle randomness in the underlying optimization problem.

As for the evaluation metric, Algorithm 3 outlines the generic procedure for computing empirical confidence rankings in a single trial. In the synthetic setting, this procedure is repeated over $T = 1 \times 10^2$ independent trials with $\ell = 1 \times 10^3$ test data points. Meanwhile, in the real-world setting, the evaluation is performed rolling over $T = 12$ periods, spanning from 2010 to 2022. Each trial uses a two-year window (24 months) of data, which is sequentially split into training, calibration, and testing sets in an 8 : 8 : 8 ratio. The reported error is the *standard error of the mean (SEM)*, computed as the standard deviation of the metric across trials divided by \sqrt{T} .

Acknowledgments

Table 7 Summary table of metrics used in the Conservativeness vs. Accuracy Tradeoff experiment.

Metric Name	Description	Mathematical Formula
Validity	The percentage of decisions where the risk estimate satisfies the conservativeness guarantee in (2) averaged across all trials.	$\frac{1}{T \cdot \mathcal{V} } \sum_{z \in \mathcal{V}} \mathbb{1} \{ \hat{\alpha}(z) \leq \alpha(z) \}$
TPR	The percentage of decisions where the method correctly identifies them to have risk of less than one, averaged across all trials.	$\frac{1}{T \cdot \mathcal{V} } \sum_{z \in \mathcal{V}} \mathbb{1} \{ \hat{\alpha}(z) < 1 \} \cdot \mathbb{1} \{ \alpha(z) < 1 \}$
MAE	The mean absolute error of the estimated compared to the true risks across all decisions and trials.	$\frac{1}{T \cdot \mathcal{V} } \sum_{z \in \mathcal{V}} \hat{\alpha}(z) - \alpha(z) $

We would like to express our sincere gratitude to [acknowledge individuals, organizations, or institutions] for their invaluable contributions to this research. We are also grateful to [mention any additional acknowledgements, such as technical assistance, data providers, or colleagues] for their support and assistance throughout the course of this work.

Algorithm 3 Empirical Confidence Ranking

Require: Original optimization $\pi^* : \mathcal{Y} \rightarrow \mathcal{Z}$; Evaluated policy $\pi : \mathcal{X} \rightarrow \mathcal{Z}$; Test dataset $\{(x_i, y_i)\}_{i=1}^{\ell}$.

```

1:  $\mathcal{Z}^* = \emptyset$ 

2: for  $i = \{1, \dots, \ell\}$  do

3:    $z_i^* \leftarrow \pi^*(y_i)$ .

4:    $\mathcal{Z}^* \leftarrow \mathcal{Z}^* \cup \{z_i^*\}$ .

5: end for

6: for  $z \in \mathcal{V}(\theta)$  do

7:    $h(z) \leftarrow$  the total occurrence of decision  $|\{i \mid z_i^* = z\}|$ .

8: end for

9: for  $i = \{1, \dots, \ell\}$  do

10:   $\hat{z}_i \leftarrow \pi(x_i)$ .

11:   $\text{rank}_i \leftarrow$  ranking of estimated decision  $|\{z' \in \mathcal{V}(\theta) \mid h(z') \geq h(\hat{z}_i)\}|$ 

12: end for

13: return Empirical confidence ranking  $1/\ell \cdot \sum_{i=1}^{\ell} \text{rank}_i$ .
```

Table 8 Summary table of baselines used in the Decision Quality Evaluation experiment

Model Name	Description	Additional remarks
PTO	<p>The standard two-stage predict-then-optimize approach (Bertsimas and Kallus 2020), which first predicts parameters and then solves the resulting optimization problem;</p> $\min_{z \in \mathcal{Z}} f(z; \hat{Y}),$ <p>where \hat{Y} is a point estimate of $\mathbb{E}[Y X]$.</p>	<p>Since X is omitted in our setting, PTO degenerates to stochastic optimization, and \hat{Y} can be simply specified as the empirical average estimator.</p>
RO	<p>Robust optimization defined as</p> $\min_{z \in \mathcal{Z}} \max_{y \in \mathcal{U}} f(z; y)$ <p>where $\mathcal{U} \subseteq \mathcal{Y}$ is the uncertainty set of Y.</p>	<p>The uncertainty set is constructed in a data-driven manner by applying naive CP to Y, using the ℓ_∞ norm residual as the nonconformity score (Zhou et al. 2024).</p>
SPO+	<p>A predict-then-optimize method where the prediction model is trained using the surrogate smart predict-then-optimize loss (Elmachtoub and Grigas 2022)</p>	<p>For each trial, it is trained for 1×10^2 epochs using a learning rate of 1×10^{-1}.</p>
DFL	<p>Decision-focused learning, where the prediction model is trained by directly optimizing the downstream objective through end-to-end differentiation of the optimization layer (Amos and Kolter 2017).</p>	<p>For each trial, it is trained for 1×10^2 epochs using a learning rate of 1×10^{-1}.</p>